Progress in Oceanography 233 (2025) 103435

Contents lists available at ScienceDirect

Progress in Oceanography

journal homepage: www.elsevier.com/locate/pocean

Temporal variability of bottom hypoxia in open and semi-enclosed coastal areas in an upwelling region

Richard Muñoz [a,f], Fabián J. Tapia [b,c,d,*], Marcus Sobarzo [b,c,d,e]

[a] Programa de Postgrado en Oceanografía, Universidad de Concepción, Concepción, Chile
[b] Departamento de Oceanografía, Facultad de Ciencias Naturales y Oceanográficas, Universidad de Concepción, Concepción, Chile
[c] Centro de Investigación Oceanográfica COPAS Coastal, Universidad de Concepción, Chile
[d] Centro Interdisciplinario para la Investigación Acuícola INCAR, Universidad de Concepción, Concepción, Chile
[e] Programa de Investigación sobre Ecosistemas del Golfo de Arauco PREGA, Universidad de Concepción, Concepción, Chile
[f] Departamento de Ecología, Facultad de Ciencias, Universidad Católica de la Santísima Concepción, Concepción, Chile

ARTICLE INFO

Keywords:
Dissolved oxygen
Temperature
Hypoxia
Coastal upwelling
Inner shelf

ABSTRACT

Hypoxia events driven by the onshore advection of oxygen-poor upwelling waters have become increasingly common along Eastern Boundary Upwelling Systems (EBUS). More frequent or intense drops in nearshore oxygen concentrations can impact the behavior, population dynamics, and geographic distribution of many coastal species. To better understand these effects, it is necessary to determine the periodicity of hypoxia in the inner shelf, its response to upwelling-favorable winds, and the local factors that may modify its intensity and duration. Here, we used a two-year record (March 2017–February 2019) of near-bottom dissolved oxygen (DO) and water temperature from seven sites spanning 260 km of the upwelling coast of Central Chile to characterize the local variability in oxygen concentration and its association with coastal winds. The temporal patterns observed in the inner shelf were compared with 13.5 years of monthly hydrographic profiles (2002–2015) from a mid-shelf station located ca. 30 km offshore. The spatial structure of nearshore hypoxia was inferred from hydrographic data gathered during two surveys conducted in winter 2018 and late summer 2019. Inner-shelf hypoxia (DO<2.0 mg/L) occurred predominantly in the austral summer and exhibited substantial among-site differences in its persistence and timing relative to wind-driven upwelling. The mean duration of summertime hypoxia events ranged between 1 and 9 days, except for a site at the innermost section of the Gulf of Arauco, where events could be as long as 62 days. Hypoxic waters appeared at the inner shelf after 1–2 days of sustained upwelling-favorable winds (59% of the hypoxia events occurred after ≤ 2 days of persistent wind). The seasonality and vertical structure of hypoxia were apparent in the mid-shelf monthly time series, with the hypoxic layer's upper limit ascending to 20–30 m depths during spring-summer (October–March) and receding to 45–60 m in autumn-winter (May–September). Hydrographic properties of the hypoxic layer pointed to Equatorial Subsurface Water (ESSW) as the source water mass for mid-shelf hypoxia throughout the year. These properties were consistent with those observed on the inner shelf. Among the seven inner-shelf sites, Arauco showed the most persistent (70% of the time spanned by our records) and severe hypoxia, with DO levels below those observed at the mid-shelf during active upwelling. We hypothesize that these conditions respond to a combination of physical phenomena and coastal eutrophication that locally enhance thermal stratification, productivity, and benthic oxygen consumption, thus amplifying the severity of hypoxia and physiological stress for marine organisms inside the Gulf of Arauco.

1. Introduction

Over the past five decades, there have been substantial changes in the heat content and oxygenation of the ocean's interior (Abraham et al., 2013; Schmidtko et al., 2017; Garcia-Soto et al., 2021). In addition to a decline in oxygen solubility due to warmer temperatures, a stronger thermal stratification of the surface ocean reduces wind mixing and ventilation, enhancing the deoxygenation effect of global warming (Deutsch et al., 2015). Also, the mid-depth ocean water masses with low oxygen content, known as Oxygen Minimum Zones (OMZ), have expanded across various ocean regions, especially along the Equatorial Pacific and the Perú–Chile coast (Breitburg et al., 2018). Along this region, as in other Eastern Boundary Currents, wind-driven

* Corresponding author.
E-mail address: ftapiaj@udec.cl (F.J. Tapia).

https://doi.org/10.1016/j.pocean.2025.103435
Received 16 April 2024; Received in revised form 30 January 2025; Accepted 6 February 2025
Available online 14 February 2025

upwelling promotes the intrusion of cold, nutrient-rich, but oxygen-deficient waters into nearshore habitats (Grantham et al., 2004; Walter et al., 2014; De La Maza and Farías, 2023).

In upwelling regions, coastal circulation is predominantly driven by Equatorward meridional winds and modified by the interaction of upwelling-driven flows with coastal bathymetry (Kirincich et al., 2005; Sobarzo et al., 2007; Figueroa and Moffat, 2000). An exposed and straight shoreline influenced only by upwelling is expected to exhibit fluctuations in near-bottom dissolved oxygen (NBO) with a periodicity similar to the cycles of intensification and relaxation of upwelling-favorable winds. In a complex shoreline, on the other hand, sections that are protected from the direct influence of upwelling (e.g., within bays) are likely to perceive changes in dissolved oxygen (DO) with different periodicity or intensity due to the interaction of upwelling-driven flows with local bathymetry, locally-enhanced thermal stratification and longer residence times of low-oxygen waters (Booth et al., 2012; Walter et al., 2014). Higher-frequency wind variability, such as diurnal sea breezes, may locally modify inner shelf circulation patterns and the cross-shelf exchange of water and its properties (Kaplan et al., 2003; Woodson et al., 2007). Furthermore, intra-seasonal modulation of thermocline depth by mesoscale features such as coastally trapped waves may modify the source depth and the physical–chemical conditions of upwelled water brought to shore (Sobarzo et al., 2016). Together, these factors induce a high degree of spatial heterogeneity in the intensity and periodicity of fluctuations in water temperature, dissolved oxygen, and other chemical properties associated with coastal upwelling (Tapia et al., 2009, 2014; Chan et al., 2017; Hernández and Tapia, 2021).

The inner shelf is a dynamic and complex environment that holds particular relevance for the life cycle of numerous species of fish and invertebrates, as well as for human activities such as fishing and aquaculture. Many pelagic and benthic species rely on the high productivity of coastal waters to harbor their early life stages, either as planktonic larvae or benthic juveniles feeding and seeking shelter in subtidal habitats. Although coastal ecosystems in upwelling regions have been exposed to sub-surface hypoxia for centuries or even millennia (Moffitt et al., 2015), the geographic extent and intensity of coastal hypoxia events appear to have increased recently (Levin et al., 2009; Altieri and Gedan, 2015). The intensification of upwelling-favorable winds along Eastern Boundary Currents (Bakun, 1990; Sydeman et al., 2014; Rykaczewski et al., 2015; Schneider et al., 2017) has enhanced the onshore advection of nutrient-rich hypoxic waters (Adams et al., 2013) and promoted increased primary productivity in some coastal regions (Vargas et al., 2007; Gutiérrez et al., 2011; Weidberg et al., 2020). Additionally, increased coastal eutrophication associated with anthropogenic activities has enhanced the deoxygenation of shallow waters due to excess organic matter, turning an increasing number of bays into “dead zones” where hypoxia is a periodic or even permanent condition (Diaz and Rosenberg, 2008).

In the eastern South Pacific, the oxygen-poor water associated with the OMZ is located at intermediate depths (100–500 m). It consists mainly of Equatorial Subsurface Water (ESSW) transported southward along the coast by the Perú-Chile Undercurrent (PCUC). The distribution of OMZ waters along the coast shows a heterogeneity strongly related to the intensity of poleward transport by the PCUC and its interaction with advective processes such as meridional jets and mesoscale eddies (Pizarro et al., 2015; Pizarro-Koch et al., 2019). In central Chile, the transport of ESSW towards the continental shelf is strongly linked to coastal upwelling, hence the correlation observed between the volume of hypoxic seawater and upwelling favorable winds in spring–summer months (September through March) (Sobarzo et al., 2007; Testa et al., 2018). During the winter (June–August), the predominant conditions of high ventilation increase dissolved oxygen levels well above the hypoxic threshold during much of this season (De La Maza and Farías, 2023). The occurrence of hypoxic events in coastal areas has a strong biological impact, modifying community structure, population sizes, and species richness, and when hypoxia is severe, triggering events of mass mortality and stranding (Hernández-Miranda et al., 2010, 2012; Aguirre-Velarde et al., 2019).

Given the ecosystem-level implications of coastal hypoxia and its prevalence along vast coastal regions influenced by upwelling, it is relevant to assess the timing and duration of hypoxic events. Understanding the oceanographic factors that drive the timing and intensity of these conditions may be of particular relevance in regions where, in addition to upwelling-driven variability, drops in dissolved oxygen concentrations reflect the influence of local factors such as eutrophication, nearshore bathymetry, and thermal stratification, which may modify the manifestation of hypoxia at the shoreline (Walter et al., 2022; Chen et al., 2021; Merma-Mora et al., 2024). In this study, we used a two-year record of near-bottom dissolved oxygen and temperature from seven sites along the upwelling coast of central Chile to assess spatial differences and commonalities in the timing of coastal hypoxia and its association with upwelling-favorable winds. A 13.5-year monthly time series from a nearby mid-shelf time series station was used to describe the monthly variability in the depth of hypoxic water and to characterize the hydrographic conditions associated with coastal hypoxia through the year. Additionally, we used dissolved-oxygen profiles from two CTD surveys across the Gulf of Arauco, the main coastal feature in the study region, to characterize the spatial extent of near-bottom hypoxia and the seasonal change in depth of hypoxic waters.

2. Data and methods

2.1. Study area

The central coast of Chile (35.5–38.0°S) encompasses one of the most productive coastal regions within the Humboldt Current System (Daneri et al., 2000; Thiel et al., 2007). Wind forcing is strongly seasonal, with a spring–summer intensification of equatorward winds and synoptic-period events of intensification/relaxation of upwelling favorable winds that typically last 3–8 and 6–7 days, respectively (Rahn and Garreaud, 2013). The Gulf of Arauco (GA) is the main coastal feature in the region, and Punta Lavapié (PLV), located at its southwestern end, is one of the two most important upwelling centers along the Chilean coast (Figueroa and Moffat, 2000; Paolini-Cuadra et al., 2004). Other embayments of a progressively smaller size (bays of Concepción, San Vicente, and Coliumo), plus two coastal islands (Quiriquina and Santa María), two submarine canyons, and coastal mountains give rise to a complex pattern of coastal winds and currents (Fig. 1) (Djurfeldt, 1989; Parada et al., 2001; Figueroa and Moffat, 2000; Sobarzo and Djurfeldt, 2004). Superimposed on the seasonal and synoptic wind variability, diurnal fluctuations associated with the sea breeze are a relevant source of local forcing that modulates inner-shelf circulation, especially in summer months (Sobarzo et al., 2010). Additionally, it has been shown that the passage of poleward-moving coastally trapped waves over the Biobío submarine canyon promotes the rise of cold, oxygen-poor canyon water and its subsequent overflow into the GA, even in the absence of upwelling favorable wind (Sobarzo et al., 2016).

2.2. Data sources

2.2.1. Mooring arrays and hydrographic surveys

Near-bottom dissolved oxygen (DO) and temperature were recorded continuously at seven inner-shelf sites spanning 260 km of shoreline (Fig. 1) using MiniDO$_2$T loggers (PME, USA) deployed along with HOBO pressure and conductivity loggers (U–24, U–20, Onset Computer, USA) at mean depths that ranged between 8 and 27 m, and at 2 m above the bottom. The MiniDO$_2$T loggers were deployed with a copper plate placed directly over the sensor (not covering the measurement area) and a copper mesh provided by the manufacturer that completely covered the surface to prevent bio-fouling and ensure data quality. Sampling intervals of 10 and 15 min were used for the

Table 1
Geographic coordinates and depths of nearshore sites from which continuous records of near-bottom oxygen and temperature were gathered. Dates of the first and latest available measurements, as well as the length of each time series, are also shown.

Site name	Latitude (°S)	Longitude (°W)	Depth (m)	Begin date (y-m-d)	End date (y-m-d)	Length (days)
Mela	36.3614	72.8708	14	2017–03–18	2019-02-20	705
Coliumo	36.5350	72.9522	10	2017–03–29	2019-02-20	694
Chome	36.7724	73.2151	27	2017–03–01	2019-02-28	730
Arauco	37.2164	73.3175	12	2017–03–01	2019-02-28	730
Llico	37.1923	73.5209	8	2017–03–18	2019-02-12	697
Piures	37.2346	73.6599	16	2018–04–07	2019-02-28	328
Yani	37.3691	73.6763	19	2017–03–29	2019-02-04	678

Table 2
Total number of days of hypoxia (d: duration) and number of hypoxia events (e) for each month of the year at the inner-shelf sites. N_h corresponds to the total duration in days (first row) and annual total hypoxia events (second row). The first and second rows of each site correspond to d and e, respectively. March 2017–February 2019.

Site	J	F	M	A	M	J	J	A	S	O	N	D	N_h
Mela	44.8	15.1	16.6	16.2	0.4	1.6	–	10.9	19.4	24.4	22.6	27.6	199.6
(14 m)	5	2	4	3	1	1	–	4	4	5	3	4	36
Coliumo	43.6	18.6	17.6	11.8	–	1.4	–	8.4	22.5	26.3	30.4	17.7	198.3
(10 m)	10	5	4	3	–	1	–	3	5	6	6	7	50
Chome	38.2	13.8	16.4	8.0	1.5	2.8	0.9	13.8	14.9	30.3	27.2	27.6	195.4
(27 m)	5	3	5	6	2	2	1	3	7	8	7	8	57
Arauco	61.8	23.8	21.3	15.8	–	–	–	–	11.0	26.5	19.9	50.9	231
(12 m)	1	2	2	3	–	–	–	–	5	6	6	3	28
Llico	16.8	8.3	9.4	0.8	–	–	–	–	0.7	17.9	0.9	8.1	62.9
(8 m)	11	4	4	1	–	–	–	–	1	10	1	10	46
Piures	9.4	5.9	2.9	2.0	0.9	0.9	1.3	0.2	–	–	2.1	1.6	27.2
(16 m)	4	4	4	1	2	1	2	1	–	–	2	3	24
Yani	10.2	1.7	3.1	13.4	3.8	–	1.5	1.4	–	3.0	2.4	5.1	45.6
(19 m)	6	1	2	9	2	–	1	1	–	5	2	4	33

oxygen-temperature and pressure-conductivity measurements, respectively. The length of each time series collected with these sensors is shown in Table 1.

Two hydrographic surveys spanning a grid of 35 stations across the Gulf of Arauco were conducted in June 2018 (winter) and March 2019 (late summer) (Fig. 1). Hydrographic profiles were gathered with an SBE–19 plus v2 CTD (Seabird Electronics, USA) equipped with a DO sensor and configured with a sampling rate of 4 Hz. Data were later processed to obtain a vertical resolution of 1 m. To contextualize the spatial and temporal variability in DO and temperature derived from our inner-shelf observations, we used data from hydrographic profiles collected monthly over 13.5 years (August 2002–December 2015) at a time-series station (Station 18, 36.50°S, 73.12°W), located ca. 30 km offshore on the mid-shelf (90 m depth) and maintained by the University of Concepción since July 2002.

2.2.2. Meteorological and satellite data

An hourly record of wind magnitude and direction was gathered through a meteorological station located on Pt. Hualpén (36.77°S, 73.21°W) at ca. 30 m above sea level. To contextualize the *in situ* wind conditions observed during the study period, a longer-term characterization of coastal wind in the region of interest was conducted using ERA5 reanalysis data (Hersbach et al., 2020). Hourly time series of zonal and meridional wind velocities spanning the period 1980–2015 were obtained for a node of the ERA5 grid closest to Pt. Hualpén, with coordinates 36.75°S and 73.50°W.

Satellite data on Sea Surface Temperature (SST) over the region of interest were acquired from available Level–3 MODIS–Aqua imagery from 2016–2019 (https://oceancolor.gsfc.nasa.gov). The spatial and temporal resolution of satellite data was 4 km and 1 day, respectively.

2.3. Data processing and analysis

Wind velocity vectors were rotated and aligned with their principal axes of variability, which were 19.4° for *in situ* winds and 12.1° East for ERA5 data. The alongshore wind stress was computed according to Harrison (1989), using a variable drag coefficient (CD) that depends on the wind speed (Trenberth, 1990). The time series of alongshore wind stress obtained from ERA5 correlated well with that obtained from *in situ* measurements at Pt. Hualpén (r^2=0.61, p = 0.013).

A climatology of alongshore wind stress in the region of interest was computed from the ERA5 data for the 1980–2015 period. Later, monthly conditions observed during 2017–2019 were superimposed on this climatology. Additionally, cumulative alongshore wind stress was computed for each spring–summer season since 1980. For this analysis, spring–summer was defined as the period between 1 September and 31 March of the following year. Trajectories of cumulative alongshore stress computed in this way for 1980–2015 were used to establish the margins of inter-annual variability in wind forcing that might be considered normal. We used the 5th and 95th percentiles of the distribution of values for each point in time during the integration period.

Dissolved oxygen and temperature data recorded with the MiniDO$_2$T sensors were quality-controlled and later converted into hourly time series. Concurrent conductivity and pressure records acquired with HOBO U–24 and HOBO U–20 sensors were processed similarly. The conductivity records were converted to salinity using the HOBO Conductivity Assistant (https://www.onsetcomp.com/resources).

Oxygen and temperature conditions were compared across the seven sites, first in terms of seasonal medians and later by comparing their median annual cycle (i.e., climatology) across sites and depths of measurement. A climatology of alongshore wind stress was computed following the same procedure. Medians were computed instead of means, considering the asymmetry of data distributions, especially in the case of dissolved oxygen and wind stress. Instead of standard deviations, the 25th and 75th percentiles were used to assess variability around the median for each month.

Hypoxia events were defined as periods when DO dropped below 2 mg/L regardless of duration, which can vary from hours to weeks (Kamykowski and Zentara, 1990; Hernández and Tapia, 2021). To detect hypoxia events and quantify their duration, hourly DO time series were first low-pass filtered to remove variability with periods

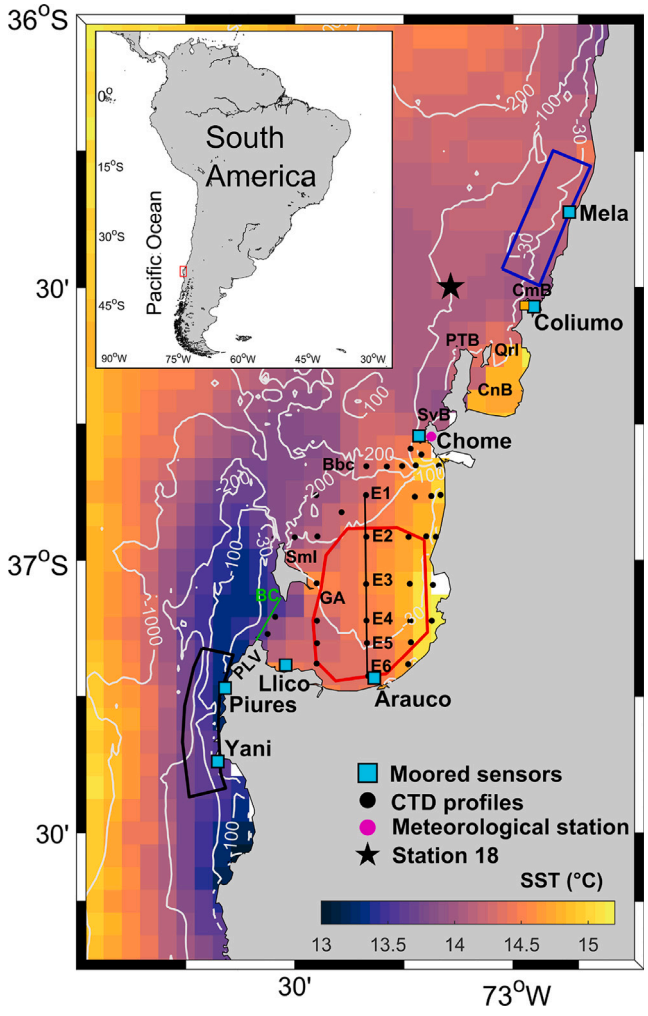

Fig. 1. Study area with the location of mooring sites (cyan squares), CTD-survey stations (black dots), Punta Hualpén weather station (pink dot), and the mid-shelf time series Station 18 (black star). The color map shows the mean field of Sea Surface Temperature (SST) computed from MODIS-Aqua data for 2016–2019. White contours show shelf bathymetry. The blue, red, and black polygons correspond to SST sub-regions used to compute monthly medians. GA: Gulf of Arauco, PLV: Punta Lavapié, PTB: Punta Tumbes, QrI : Quiriquina Island, SmI: Santa Maria Island, CmB: Coliumo Bay, Cnb: Concepción Bay, SvB: San Vicente Bay, Bbc: Biobío canyon, and BC: Boca Chica. See Table 1 for more details.

<40 h (inertial, diurnal, semi-diurnal, and higher frequencies). The number of hypoxia events and their duration (in days) were then computed by month. To assess their association with changes in wind forcing, cumulative wind stress before each event was computed from the hourly time series of alongshore stress. Previously, and to be consistent with the DO time series, the wind was low-pass filtered with a 40 h cutoff. The integration period used to compute cumulative wind stress before a hypoxia event was defined based on the sign changes in the alongshore wind component. Positive values for meridional wind stress (upwelling favorable) were integrated from the onset of a hypoxia event (DO<2.0 mg/L) back to the nearest zero-crossing.

To characterize seasonal and inter-annual changes in the occurrence and vertical structure of hypoxia at the mid-shelf (90 m depth), we used the CTD-O profiles of the Station 18 time series collected between 20 August 2002 and 22 December 2015 to track the depth of the hypoxic layer's upper limit (i.e., minimum depth with DO<2 mg/L) and to examine temporal patterns in the hydrographic features (temperature, salinity, density) of water inside the hypoxic layer. The original database consisted of 352 profiles with 1-meter vertical resolution, gathered on 152 visits to Station 18 during the above-mentioned period. A time-averaged profile was obtained when several profiles were collected during the same day (often between 6 AM and 3 PM). Oxygen data from the CTD-O sensor were corrected using Winkler-titration measurements on water samples collected from 6 depths (0, 10, 20, 30, 50, 80 m). For each of these 152 CTD-O profiles, we found the hypoxic layer's upper limit through linear interpolation. To characterize the hydrographic properties of hypoxic waters and assess their seasonal changes, from each profile we collected all T-S data below the upper boundary of hypoxia. These data were used to compute the mean temperature of the hypoxic layer and to produce a T–S diagram where points were color-coded by the month of sampling.

To examine the spatial coverage of hypoxia in the Gulf of Arauco, horizontal distributions of near-bottom oxygen concentrations were mapped using the hydrographic profiles gathered in June 2018 (early winter) and March 2019 (late summer). Additionally, the spatial change in depth and thickness of the hypoxic layer was examined using a subset of the hydrographic profiles along a North-South transect in the center portion of the Gulf (E1—E6, see Fig. 1). As in the analysis of CTD profiles from Station 18, T-S diagrams were constructed to examine potential patterns in the conservative properties (temperature, salinity, and density) of hypoxic water reaching the Gulf and its innermost section.

3. Results

3.1. Statistical description of wind, temperature, and oxygen variability

During the two years of study (March 2017–February 2019), coastal wind stress showed the seasonal pattern typically observed for this latitude, with intense and persistent southerly winds in spring–summer and predominantly northerly winds in the fall-winter months (Fig. 2a). The two years spanned by our study exhibited contrasting patterns of alongshore wind stress during the spring and early summer months. Although for both seasons, the monthly medians of alongshore wind stress fell within the interquartile range computed for 1980–2015 (Fig. 2a), the cumulative wind stress trajectories computed for spring and early summer months were lower in 2018–2019 than in the previous season, i.e., the spring of 2018 was not as windy as the previous one (Fig. 2b). The time series of alongshore wind stress measured at Pt. Hualpén showed more intense southward winds starting in May (i.e., autumn). The largest events were recorded during the first winter, June 2017, and July of the following year (Fig. 3a). Southwesterly winds, favorable to coastal upwelling, became dominant in late winter to early spring (September–October) and were stronger in the spring of 2017 (Figs. 2b, 3a).

The variability of near-bottom temperatures (NBT) was coherent with seasonal- and synoptic-scale changes in wind forcing at all study sites (Fig. 3b–h). A sustained drop in NBT from April–May to September of both years, with predominant northerly winds, was attributable to a heat loss during austral winter rather than the upwelling of cold subsurface waters. More intense episodic cooling occurred from September onwards, especially from October 2017 to January 2018, when southwesterly winds were more intense than from October 2018 to January 2019. During spring–summer, these coastal cooling periods alternated, in some sectors more than in others, with warm events due to the onshore advection of warmer surface waters during wind relaxation. The near-bottom oxygen (NBO) also showed a seasonal signal, although it was less clear at the sites located south of Pt. Lavapié, namely Piures and Yani (see Section 3.4).

In most cases, the NBO variability appeared to be strongly influenced by synoptic and inter-monthly fluctuations associated with the change in winds. It was tightly coupled with temperature fluctuations during spring–summer months, especially between October and January, at sites north of Llico (Fig. 3b–f). Minimum DO values at these sites occurred mainly during the spring–summer season (Fig. 3b–h).

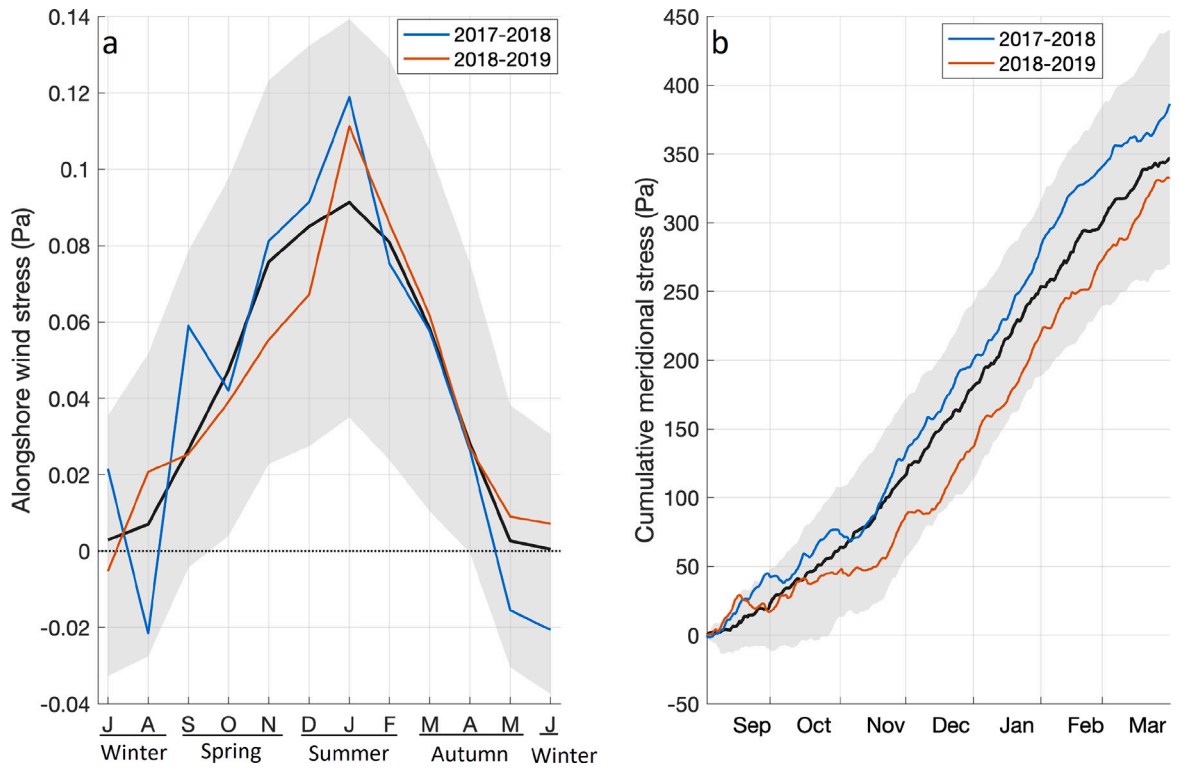

Fig. 2. Comparison of alongshore wind conditions observed for Pt. Hualpén during the two spring–summer seasons for which *in situ* data were collected (2017–2018 and 2018–2019, blue and orange lines) compared with the 1980–2015 climatology computed from ERA5 data. (a) Monthly medians computed for the two sampling seasons overlaid on the climatological medians (black line) and percentiles 25 and 75 (shaded area). (b) Trajectories of the cumulative alongshore wind stress during spring–summer (from 1 September until 31 March of the following year) for each of the two study seasons (color lines), superimposed on the median trajectory for 1980–2015 (black line) and percentiles 5 and 95 (shaded area).

Although all loggers were deployed ca. 2 m above the bottom, the among-site differences in mooring depth appeared to introduce a small bias in terms of the highest temperatures and DO levels that could be recorded during the spring–summer months (Fig. 4), with significant negative correlations between site depth and the 99th percentiles of NBT (Spearman's r=−0.96, p<0.001) and NBO (Spearman's r=0.86, p = 0.014). The warmest temperature recorded during the spring–summer at the shallowest site (Llico) was ca. 2 °C higher than the highest values recorded at the deepest site (Chome). Similarly, the highest DO values recorded at Llico were 1.9 mg/L higher than those recorded at Chome. These clear and strong correlations were not observed during autumn–winter (Fig. 4a–b). In addition to local depth, among-site differences in median NBO appeared to depend strongly on the season and the site's location relative to shoreline features such as Pt. Lavapié. The distributions of NBO were similar among sites during the autumn–winter months, with median DO concentration between 5 and 7 mg/L (Fig. 4b). In the spring–summer, there were apparent differences in the median and spread of NBO values around the median. Sites Arauco and Chome exhibited the lowest median NBO and the most asymmetric distributions, with over 50% of the recorded DO values below 2 mg/L. These two sites also exhibited the greatest contrast between seasons, with non-overlapping interquartile ranges (Fig. 4b). At all sites, the median NBO in spring–summer was lower, and the range of values was wider than in autumn–winter. The NBT showed smaller seasonal differences than observed for NBO. In autumn–winter, temperatures were higher than in spring–summer at most sites, with differences of less than 1 °C. Only Llico, the shallowest site, displayed a different pattern, with higher spring–summer temperatures and lower autumn–winter temperatures (Fig. 4a).

3.2. Characterization of hypoxia events

The persistence of hypoxia, quantified as the percentage of total measuring time with DO<2 mg/L, was highest at site Arauco in January (99.7%) and December (82.1%), indicating that during this period, near-bottom waters are in a quasi-permanent state of hypoxia (Fig. 5b). During the same period, hypoxia was substantially less persistent at southern sites. On the other hand, between May and August (autumn–winter), sites Arauco and Llico were not exposed to hypoxia. Although Llico and Arauco are in the Gulf's innermost section and close to each other (20 km), hypoxia events in Llico were much shorter than in Arauco. Llico is a shallower site, more strongly influenced by the exchange of ventilated surface water through the Gulf's southern opening known as Boca Chica (see Fig. 1).

The mean duration of hypoxia events computed by month and location revealed that Arauco exhibits the longest exposure to hypoxia between December and March, with an annual mean of 14.6 days (Fig. 5a). Sites Chome, Coliumo, and Mela – in the northern section of the study region – had mean durations that ranged between 3.1 and 5 days. South of Arauco, on the other hand, hypoxia events were 2–5 times shorter, with mean durations of at most 1.3 days (Fig. 5a).

The total number of hypoxia events per site ranged between 28 in Arauco and 57 in Chome (excluding site Piures, given the shorter data record). The total exposure to hypoxia was longer at Arauco and sites further north than at sites Llico and Yani. Thus, the site with the fewest hypoxia events (Arauco) displayed the longest exposure because events at this site were, on average, much longer than at other sites during the summer months (December–March). During the same months, hypoxia events were much shorter at sites north of Arauco (Chome, Coliumo, Mela), with average durations of 3.5–6.9 days in December and 4.4–9.0 days in January (Table 2).

3.3. Response of NBO to wind stress during the upwelling season

Regardless of the duration and intensity of hypoxia events, their onset was preceded by persistent upwelling-favorable winds. In general,

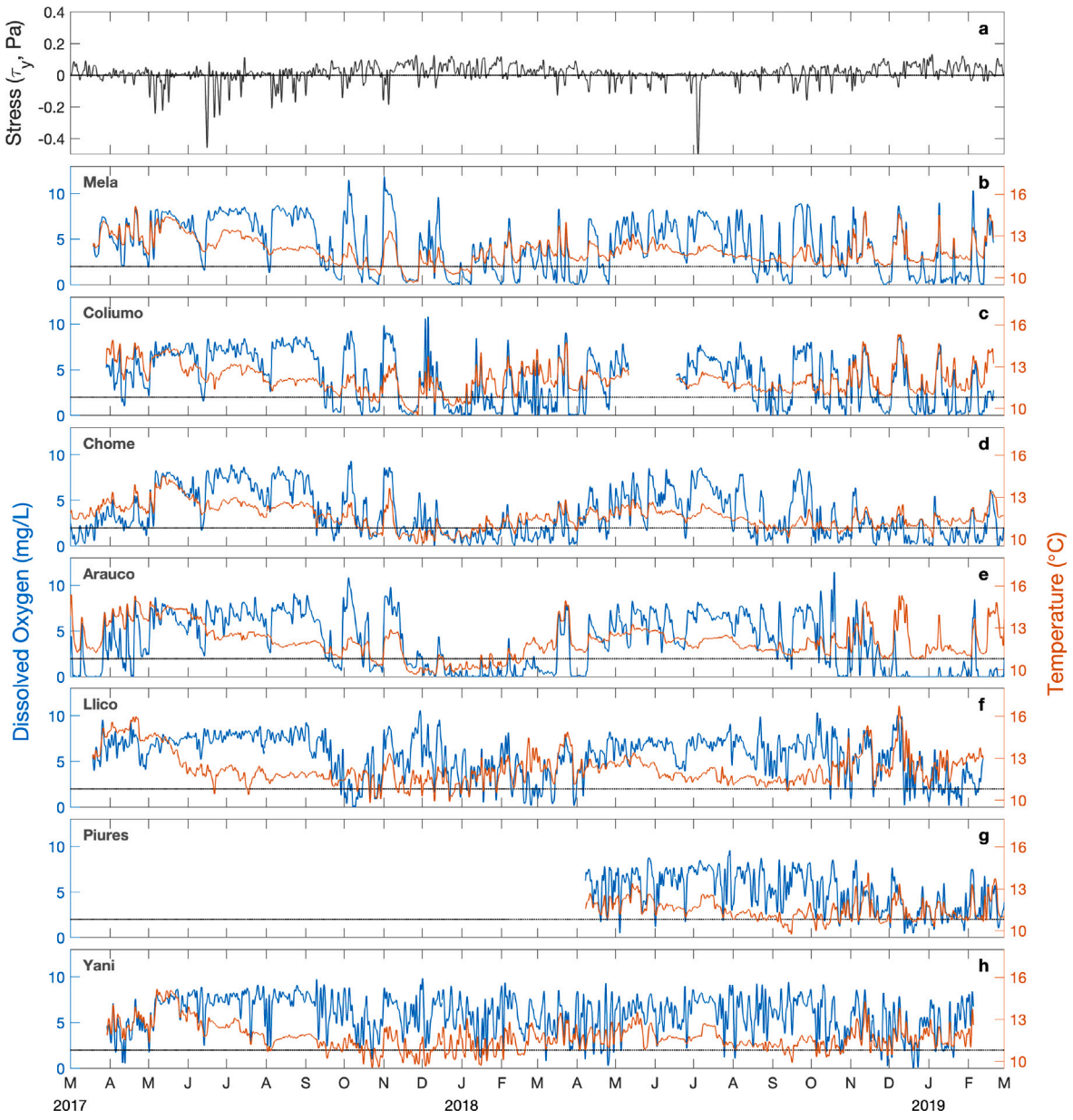

Fig. 3. Subinertial time series. (a) Alongshore wind stress at Pt. Hualpén, (b-h) near-bottom dissolved oxygen (blue) and near-bottom temperature (orange) at the seven sampling sites. Gray horizontal lines indicate a dissolved oxygen concentration of 2.0 mg/L, which is used here to define hypoxia. Positive values in (a) indicate upwelling-favorable winds.

most hypoxia events (59%) were preceded by ≤ 2 days of sustained upwelling-favorable wind stress, with average intensities of 0.6–1.1 Pa (Fig. 6). Only at sites Chome and Yani were more hypoxia events associated with shorter or longer periods of sustained wind stress (1 and 4 days, respectively; Fig. 5). Of the 274 hypoxia events in our data, 188 (68.6%) occurred after ≤ 5 days of sustained upwelling-favorable wind.

The average NBT and NBO computed during the hypoxia events exhibited significant spatial differences (Fig. 6). For example, the NBT-NBO diagrams for Mela, Chome, Yani, and Piures (exposed sites) revealed that hypoxic conditions at these sites are restricted to a narrow thermal band between 10 °C and 12 °C (Fig. 6a, c, f, g). At less exposed sites such as Coliumo, Arauco, and Llico, hypoxia was associated with higher temperatures (NBT >12 °C, Fig. 6b, d, e). The most severe hypoxic conditions (NBO <0.5 mg/L) were registered at Arauco and Coliumo (Fig. 6b, d). The coefficient of variation for NBT at Arauco (CV = 9.7) showed that hypoxia at this site is associated with a wider temperature range than at other sites (9–14 °C). On the other hand, Yani corresponded to the site with the lowest temperature variability associated with hypoxia (CV = 3.3).

3.4. Seasonal and yearly variability of NBT and NBO

Near-bottom temperature (NBT) and oxygen (NBO) exhibited distinct seasonal cycles at most sites, with more similarities among sites for NBT than for NBO and with clear differences in the timing of minimum values for temperature (September) and dissolved oxygen (October onwards) (Fig. 7). Although surface temperatures inside the Gulf of Arauco and farther North (red and blue polygons in Fig. 1) began to increase in October and reached maximum values in February, following the seasonal cycle of solar radiation, NBTs (solid lines in Fig. 7a) remained cool from September to January (March in the case of Piures). They rose from February–March until May, which was, on average, the warmest month at all but one site (Llico). The monthly median temperatures at 30 m depth on the mid-shelf (Station 18) were consistent with the bottom temperatures recorded at our inner-shelf

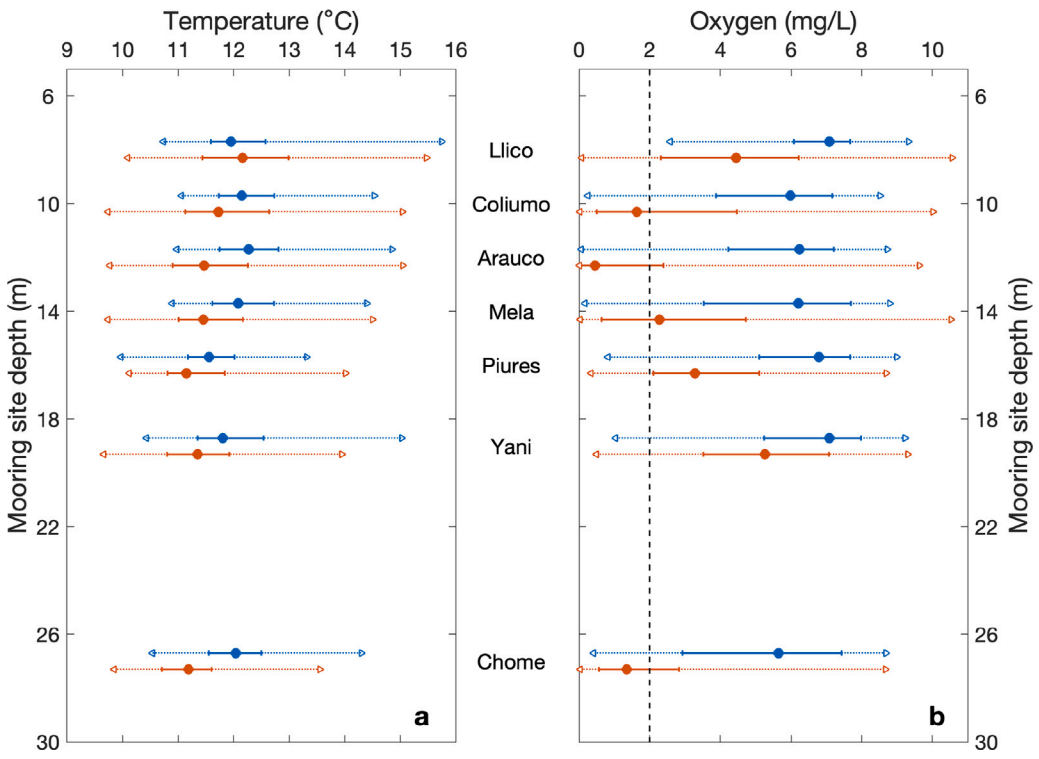

Fig. 4. Variability of near-bottom temperature (a) and dissolved oxygen (b) by season and site sorted by mooring depth. Medians and interquartile ranges are shown as filled circles and horizontal bars for spring–summer (orange) and autumn–winter (blue). The range spanned by data on each season and site (dotted lines) is represented by percentiles 1 and 99 (triangles). The vertical dashed line in (b) indicates the threshold for hypoxia considered in this study (DO=2 mg/L).

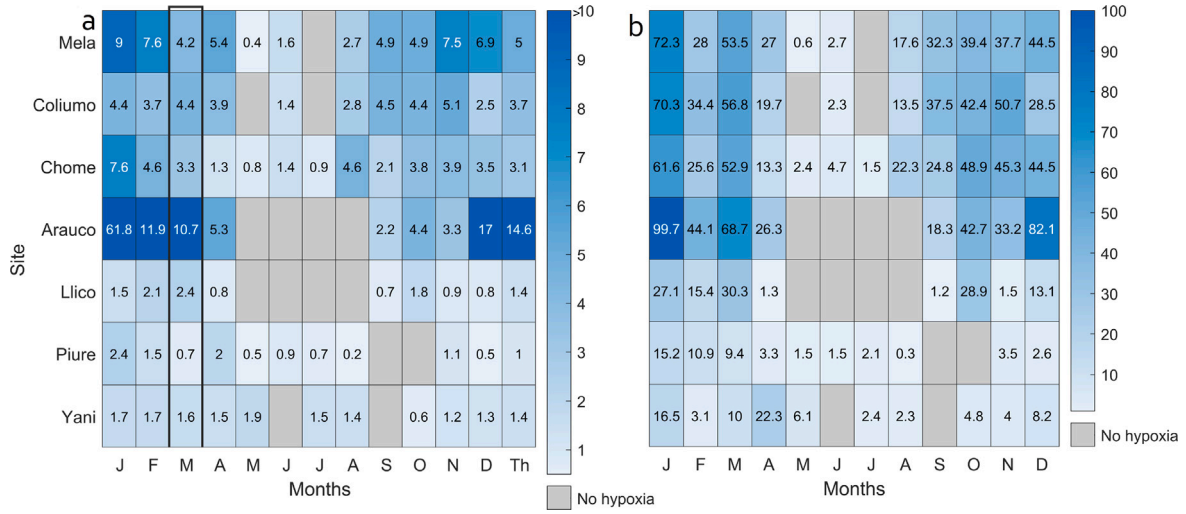

Fig. 5. (a) Mean duration (in days) of hypoxia events by month and site. Each cell corresponds to the total number of days of hypoxia divided by the number of hypoxia events detected on each calendar month. Th is the annual mean duration per site. (b) Monthly occurrence of hypoxia (as a percentage relative to the total number of days per month). March 2017–February 2019.

sites (dashed line in Fig. 7a). A similar seasonal pattern was observed for SST in a coastal area south of Pt. Lavapié (black polygon in Fig. 1), where the surface-cooling signal from this upwelling center is perceived more strongly.

The monthly NBO medians remained at their highest level (6.5 to 7.5 mg/L) during the winter (Fig. 7b), dropped rapidly in early spring (September–October) with the increase in southwesterly winds, and remained below 3 mg/L from November through March in Arauco, Chome, and Coliumo, and from November through January in the case of Mela. These sites generally adjusted well to the seasonal cycle observed at 30 m depth on the mid-shelf (dashed line in Fig. 7b). A seasonal change was less apparent at Llico and Piures and not detected at Yani. Monthly NBO medians at Piures, Yani, and Llico, located in the southern section of the study area, did not go below 2.0 mg/L.

The monthly hydrographic data collected from Station 18 between 2002 and 2015 provided a canonical mid-shelf seasonal pattern to use as a baseline to interpret our inner-shelf data. Additionally, it revealed the seasonality and inter-annual variability in the hypoxic layer's upper limit (Fig. 8a), which varied between depths of 50–60 m in winter (June–August) and 20–30 m in spring–summer (October–March) and

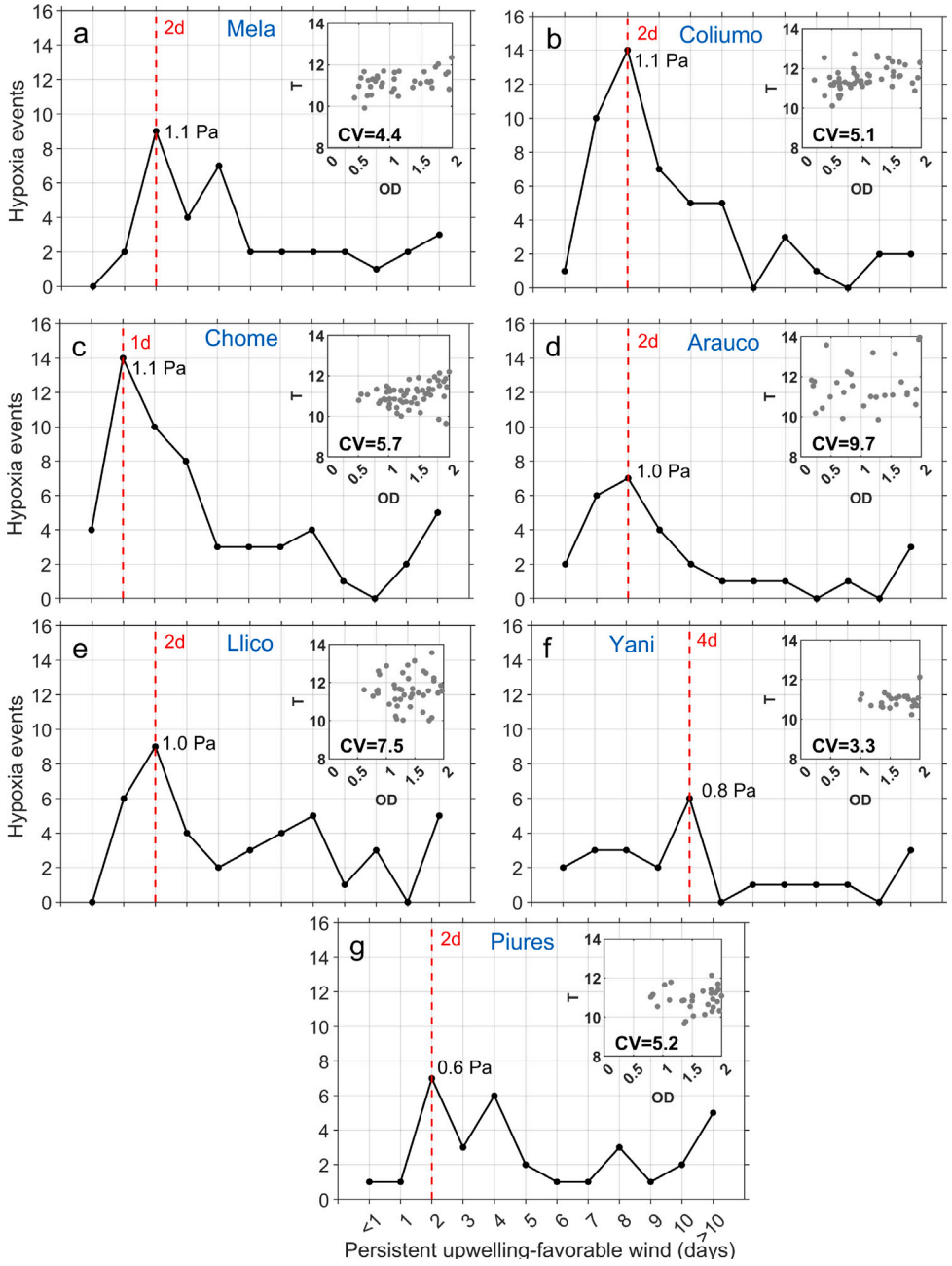

Fig. 6. Distribution of days with persistent alongshore wind stress before hypoxia events for each sampling site. The vertical dashed red line shows the cumulative wind days that generated the highest hypoxia. Black numbers show the average cumulative wind stress (Pa). Small panels show the relationship between oxygen and temperature values averaged during each hypoxia event. The coefficient of variation (CV) is shown in the lower-left corner of each small panel. CV = (standard deviation (NBT) / average (NBT)) x 100.

early autumn (April) (Fig. 8b). Temperatures in this hypoxic layer were lowest (< 9.5 °C) between spring and early summer (September–December) and increased to 11–12 °C through autumn and winter (April–July) without a large change in salinity (Fig. 8c), thus remaining within the range of T–S (T< 11.5 °C, S≥34.5) and density values known for Equatorial Subsurface Waters (ESSW) in this region (Sobarzo et al., 2007).

3.5. Hypoxia in the Gulf of Arauco

High-resolution hydrographic data collected across the Gulf of Arauco provided a way to compare the spatial structure of hypoxia in late summer (March 2019) and early winter (June 2018). In late summer, the bottom area covered by hypoxic water was approximately 1030 km^2. These bottom waters were associated with low temperatures (11.8 °C) and high salinity (34.6) and with the 26.3 isopycnal, which followed the 25 m isobath (Fig. 9a). NBO levels > 2 mg/L were observed at only two shallow coastal sites (depth<15 m): Escuadrón on the NE Gulf (NBO > 4 mg/L) and Tubul-Llico on the SW section (NBO > 5 mg/L). During winter, near-bottom hypoxic waters were associated with less dense waters (σ = 26.0–26.2), with temperature and salinity of 12.0 °C and 34.3–34.4, respectively. The area spanned by near-bottom hypoxic waters decreased to 879 km^2 (Fig. 9b). In general, bottom hypoxia in the Gulf of Arauco was associated with denser water and spanned a larger area in summer than in winter.

The vertical distribution of dissolved oxygen along a meridional transect from the Gulf's head to the southern rim of the Biobío Canyon (stations E6 to E1 in Fig. 1a) showed that during the late summer

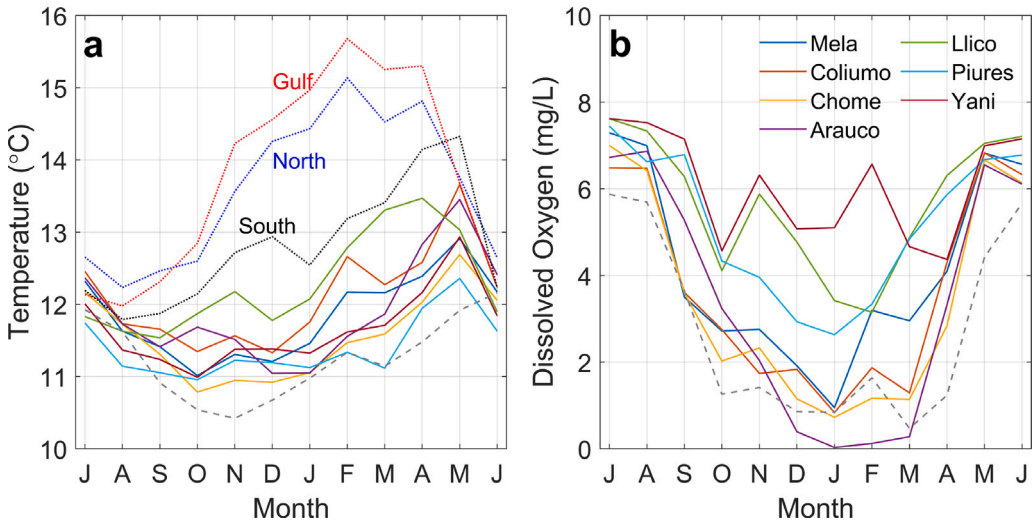

Fig. 7. Summer-centered climatologies for near-bottom temperatures (NBT) and dissolved oxygen (NBO) at the inner-shelf sites (solid lines). (a) Monthly medians of NBT and MODIS-derived SST (dotted lines) for the three sub-regions shown in Fig. 1. (b) Monthly medians of NBO (solid lines). Dashed gray lines in (a) and (b) correspond to monthly medians for data from 30-m depth at Station 18 (2002–2015).

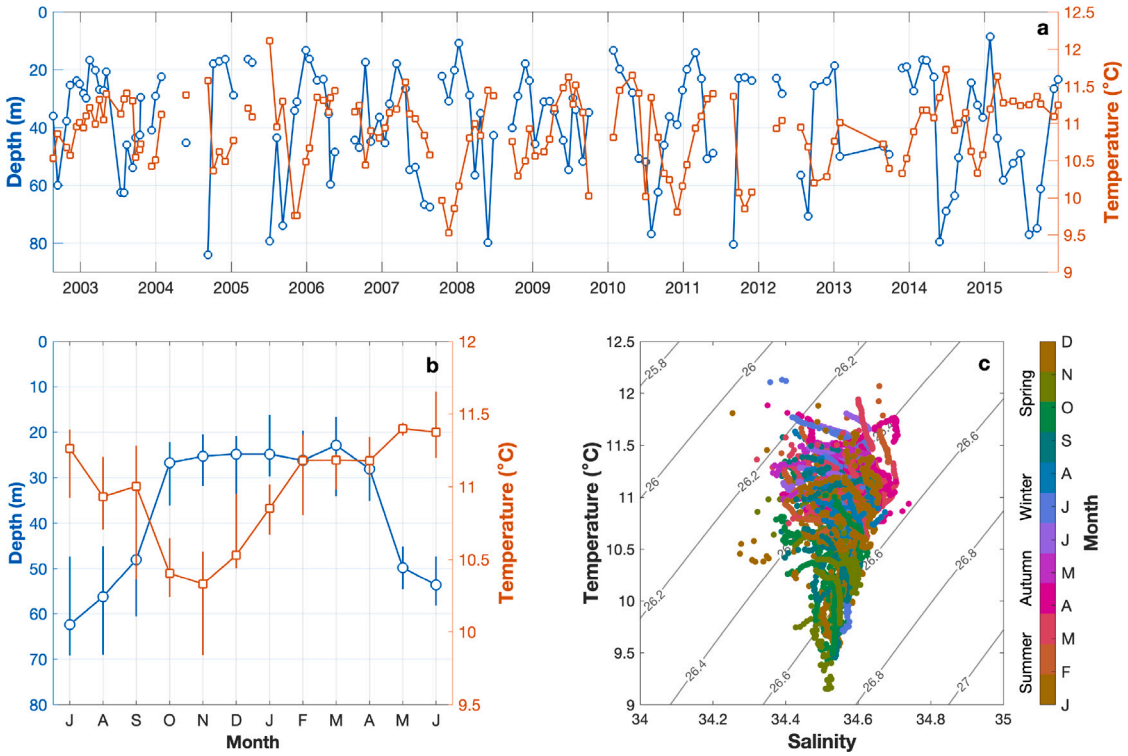

Fig. 8. Temporal variability in the depth of the hypoxic layer's upper limit (i.e., minimum depth with DO<2 mg/L) and the mean temperature of hypoxic waters at the mid-shelf time series Station 18 (2002–2015). (a) Depth of the hypoxic layer's upper limit (blue) and depth-averaged temperature below this depth (orange), (b) Summer-centered climatology of the upper limit's depth (blue) and the temperature of hypoxic waters (orange), and (c) T/S diagram for hypoxic waters (DO< 2 mg/L) color-coded by month. Contours in (c) indicate isopycnals. Symbols in (b) correspond to the monthly medians, and the error bars show the 25th and 75th percentiles of the data for each month.

of 2019, the hypoxic layer's upper limit ranged between depths of 20 m at the canyon's rim to 10 m at the Gulf's head, near site Arauco. During winter 2018, the hypoxic layer's upper limit fluctuated between depths of 40 m at E2 and 30 m at E5 (Fig. 10c). Although these surveys represent only snapshots of late summer and winter conditions, the hypoxic layer's upper limit at E1 (i.e., the Gulf's deepest section) was found at depths consistent with those observed during the same time of year at Station 18 for over a decade (see Fig. 8b). The T–S diagrams for the E1-E6 transect during these two surveys showed that hypoxia is associated with a wider temperature range in summer, while salinity is restricted to values close to 34.5 (Fig. 10b). On the other hand, in the winter, the range of temperatures is narrower, but salinity varies widely, including water in the upper section of the hypoxic layer (Fig. 10d). Finally, the seasonal difference in isopycnals associated with hypoxia in the Gulf of Arauco hypoxia, with σ values of 26.1–26.4 in summer and 26.0–26.2 in winter, indicated that inner-shelf hypoxia is strongly influenced by the advection of Equatorial Subsurface Waters (ESSW) from mid-shelf upwelling, especially in the summer.

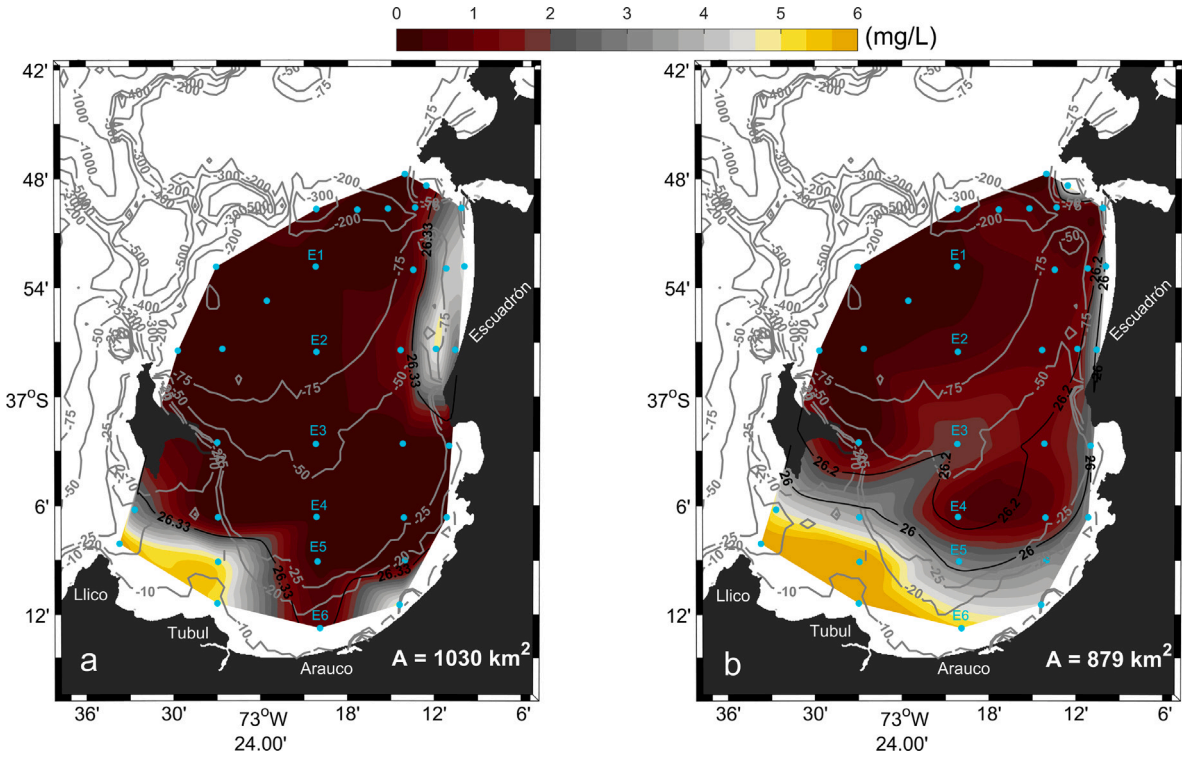

Fig. 9. Horizontal distribution of dissolved oxygen (mg/L) at the bottom of the Gulf of Arauco for (a) Late summer and (b) Winter. The gray lines are isobaths, and the color palette shows dissolved oxygen concentration. Thicker black lines correspond to the isopycnals associated with the hypoxic layer's upper limit. The stations in the center of the area (E1–E6) correspond to the T–DO profiles plotted in Fig. 10. White letters indicate the area (km^2) affected by hypoxia.

4. Discussion

Eastern Boundary Upwelling Ecosystems are widely known for their high productivity levels and critical role in the ocean-atmosphere exchange of greenhouse gases. Their response to climate-driven changes in atmospheric forcing and the interaction between upwelling intensification and changes in the chemistry of the ocean's interior has attracted much attention over the past two decades. Ocean deoxygenation is undoubtedly one of the most consequential changes for marine ecosystems. Large sections of the ocean's interior where dissolved oxygen (DO) levels fall below 2 mg/L, known as Oxygen Minimum Zones (OMZ), have expanded by 4.5% in the last decades (Breitburg et al., 2018). One such region extends across the Eastern Equatorial Pacific and southwards along the west coast of South America, spanning the Perú-Chile coast down to 37–38°S (Fuenzalida et al., 2009; Pizarro-Koch et al., 2019) and occasionally reaching latitudes of 44–45°S (Silva and Vargas, 2014; Linford et al., 2024). The coast of central Chile is thus embedded in a section of the Humboldt region strongly influenced by the OMZ, spanning depths of 100–400 m depending on the latitude (Fuenzalida et al., 2009; Pizarro-Koch et al., 2019). On the Concepción coast (36.5°S), the OMZ's zonal position has been shown to change seasonally: on the continental shelf in the summer and farther offshore in the winter (Pizarro et al., 2015). This seasonal displacement is likely to underlie the seasonal fluctuations in the thickness of the hypoxic layer reported in our study.

Although the upper boundary (minimum depth) of the OMZ fluctuates seasonally in response to seasonal wind forcing, which is mainly controlled by a latitudinal displacement of the South Pacific Anticyclone (Schneider et al., 2017), the monthly data from the continental shelf off Concepción (Station 18) show that the bottom waters of the continental shelf are permanently hypoxic, except for some short instances in winter months when the bottom water experiences enhanced oxygenation and the upper boundary of the OMZ deepens (De La Maza and Farías, 2023). During coastal upwelling, oxygen-poor waters can rise to depths <20 m and reach shallow coastal sites (Sobarzo et al., 2007; Hernández-Miranda et al., 2010). These subsurface waters are typically cold, with high concentrations of nutrients that fertilize the photic zone and enhance primary production (Daneri et al., 2000; Jacob et al., 2018). The rise and onshore advection of these oxygen-poor waters are mediated mainly by the coastal upwelling process and modulated by the bathymetry, particularly by local submarine canyons (Sobarzo et al., 2007; Vergara et al., 2024). Therefore, the intensification of upwelling favorable winds in the SE Pacific and other EBUS regions (Sydeman et al., 2014; Belmadani et al., 2013; Winckler Grez et al., 2020) is expected to promote the expansion of low-oxygen coastal areas and the increase in the frequency of hypoxia events, with negative impacts on marine ecosystems (Bakun et al., 2015; García-Reyes et al., 2015). At the same time, larger-scale deoxygenation in a warmer and more strongly stratified ocean (Diaz, 2001; Breitburg et al., 2018) is a cause for great concern due to the potential adverse impacts on ecosystems and biogeochemical cycles (Keeling et al., 2010; Limburg et al., 2020).

Thus far, most of the research on coastal hypoxia in Chile has been focused on the mean, long-term patterns (Fuenzalida et al., 2009; Levin et al., 2009), seasonal and interannual fluctuations (Silva and Vargas, 2014; De La Maza and Farías, 2023), and the ecological impacts of specific hypoxia events (Levin et al., 2009; Hernández-Miranda et al., 2012; Ruz et al., 2018). Analyses of DO temporal variability and hypoxia based on continuous records at multiple sites have been lacking for this region and have only recently been reported in the literature worldwide (e.g., Herrera-Becerril et al., 2022; Merma-Mora et al., 2024). Our study is the first to use such a dataset from multiple inner-shelf sites to focus on hypoxia events taking place over 260 km of the central Chile coast. Our statistical characterization of hypoxia events at multiple sites, their seasonality and spatial differences, and their association with upwelling conditions contribute to the finer-resolution understanding of coastal hypoxia and its driving factors. Technological advances in the continuous monitoring of dissolved oxygen have allowed a closer look at high-frequency and small-scale variability (Silva

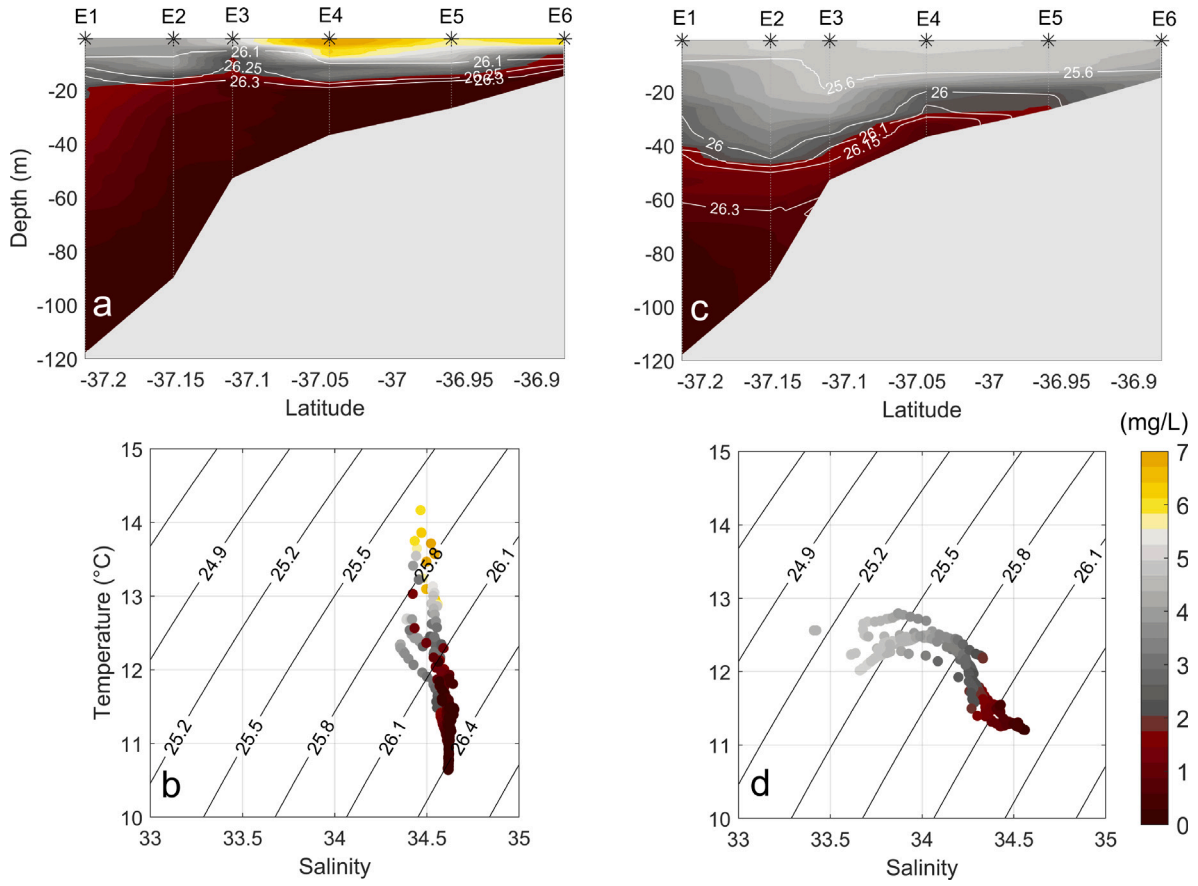

Fig. 10. Hydrographic section of dissolved oxygen (mg/L) during two cruises in the Gulf of Arauco (stations E1 to E6, see Fig. 9). (a) March 2019 (late summer), and (c) June 2018 (winter). The black asterisks at the top indicate the location of each profile. The depth of each profile is shown with vertical gray dots. The white contours indicate isopycnals with their respective value. The T–S diagrams for the March 2019 and June 2018 cruises are shown in panels (b) and (d), respectively. The color palette shows hypoxic concentrations (DO<2.0 mg/L) in red.

et al., 2022), providing a more detailed picture of how DO changes at scales that are probably critical for the physiology and behavior of marine organisms.

The spatial resolution and temporal coverage of our records made it possible to visualize differences in the recurrence and duration of hypoxia events, as well as in the seasonality of near-bottom temperature and dissolved oxygen among sites that are only tens of kilometers apart. First, although all sites exhibited a clear seasonal signal in near-bottom temperatures, with the lowest temperatures in spring (September–December) and the warmest waters in autumn (April–May), there were clear spatial differences in mean levels (Fig. 7a). Llico was consistently warmer than all other sites due mainly to a shallower mooring depth and the consequently stronger influence of solar radiation. On the other hand, sites Yani, Piures, and Chome – the three deepest moorings – were consistently colder than all other sites in autumn–winter but not always the coldest during the spring–summer (Fig. 7a). Despite the clear seasonal pattern in temperatures, sites Llico and Yani lacked a clear seasonal signal in DO, with median levels higher than at all other sites during the spring–summer (November–March). This anomaly is likely due to greater vertical mixing induced by differences in the exposure to strong currents, wave action, and/or local wind mixing. Llico is notably the shallowest of all sites, located near the Gulf's southern opening (Boca Chica), which is a shallow (<20 m depth) and narrow area (ca. 9 km) between Point Lavapié and the southwestern tip of Isla Santa María (see Fig. 1). Currents are strong near this site, and water is actively exchanged with the open ocean (Valle-Levinson et al., 2003). A recent study conducted in the area (Contreras-Rojas et al., 2024) gathered ADCP data from Boca Chica during autumn–winter (May–July 2018) and early spring (September 2016). It shows that, in both seasons, there is a net outflow throughout the water column at Boca Chica, with mean current velocities that range (from bottom to surface) between 3–13 cm/s in early spring and 4-9 cm/s in autumn–winter. Yani, on the other hand, is located in the section of the study region where the continental shelf is narrowest, and surface waters are consistently colder due to upwelling at Pt. Lavapié (see Fig. 1). Thus, we expected Yani and the nearby Piures to register the lowest temperatures and DO levels among all sites, especially during spring–summer. However, the Yani mooring was deployed near the mouth of a small SW-facing cove, exposed to strong SW winds and wave action throughout the spring–summer season. It must be noted that although the DO concentrations at Yani appeared higher than at other sites during the spring–summer, the oxygen saturation levels during the same period varied between 10%–20% and stayed below 30% throughout the year (data not shown). These saturation levels are comparable to those observed at 30-m depth on the mid-shelf (Station 18) during the upwelling season.

The events of inner-shelf hypoxia identified in this study were strongly associated with equatorward wind stress, typically blowing persistently for 1–2 days before the onset of hypoxia (see Fig. 6). Thirty-eight percent of all hypoxia events recorded in the two years of study were preceded by 1–2 days with persistent upwelling-favorable wind. This temporal scale for the delay between the onset of upwelling and the occurrence of inner-shelf hypoxia is consistent with the order of magnitude of the vertical velocities estimated from continuity considerations in the study area (U/L = W/H). Here, U, L, H, and W correspond to the typical horizontal velocity scales (U), distance from Station 18 to shore (L), depth of the hypoxic layer's upper limit (H), and vertical velocities (W), respectively. Taking U = 0.2 m/s, L = 30 km, and H =

30 m, the order of magnitude of W is 0.2 mm/s (Johnson, 1977). For these values, the rise of hypoxic waters toward the inner shelf would take 1.7 days.

Hypoxia was most severe at site Arauco, located in the Gulf's innermost section, particularly between December and March when NBO concentrations were lower than measured at greater depths on the mid-shelf (Fig. 7b) and temperatures were slightly higher (11–12 °C vs. 10.5–11 °C, see Figs. 7a and 8b). Considering that this site might not be the only section of the Gulf's coast with oxygen conditions as extreme as those documented here (see Fig. 9), a discussion of the factors contributing to the intensification of hypoxia at Arauco is warranted. First, Wong et al. (2021) and Mardones et al. (2022) have shown that residence times near the Arauco site may increase (up to 15 days) during periods of upwelling relaxation in the summer, which may partly explain the nearshore increase in temperatures and locally intensify DO limitation due to low water renewal. Additionally, the development of an upwelling shadow (sensu Graham and Largier, 1997) in the Gulf of Arauco during spring and summer (Wong et al., 2021) can increase thermal stratification and hamper the ventilation of bottom waters, which would further enhance DO limitation (Atkinson et al., 2002; Largier, 2020; Diaz, 2001), especially in an area that is known for its high levels of productivity and phytoplankton biomass (Valle-Levinson et al., 2003), where high loads of organic matter and oxygen demand at the bottom are expected. A third physical phenomenon that must be mentioned here is the passing of coastally trapped waves, which have been shown to interact with the Biobío submarine canyon and cause the rise – and potential onshore advection – of cold hypoxic waters even in the absence of wind-favorable wind (Sobarzo et al., 2016; Saldías and Allen, 2020; Saldías et al., 2021; Sahu et al., 2022).

Finally, in addition to the natural inputs of nutrients and organic matter, anthropogenic inputs from multiple urban and industrial activities (e.g., agriculture, forestry, fishing ports, sewage outfalls) converge along the Gulf of Arauco (e.g., Ahumada et al., 2004; Aguirre Martínez et al., 2009; González-Saldía et al., 2019; Cid Aguayo et al., 2019; Chandia et al., 2022) and have the potential to intensify or prolong hypoxic conditions in near-bottom waters. The occurrence and magnitude of these effects are topics to consider for future investigations of coastal hypoxia and the factors driving its spatial–temporal variability.

5. Conclusions

We have shown that the timing of inner-shelf hypoxia along the study region is consistent with the seasonality and timing of wind-driven upwelling on the mid-shelf. The forcing of inner-shelf hypoxia by the onshore advection of hypoxic waters from upwelling is further supported by the shared T–S properties, indicative of a common water mass of origin (ESSW), between the mid-shelf and inner-shelf bottom waters.

The monthly time series gathered from the mid-shelf Station 18 between 2002 and 2015 revealed that the hypoxic layer varies seasonally in a way consistent with the onshore/offshore displacement of the OMZ reported by previous studies (Pizarro et al., 2015). This seasonal thickening/thinning of the hypoxic layer on the mid-shelf translates into waters with DO<2 mg/L ascending to 20–30 m depths during spring–summer (October–March) and receding to 45–60 m in autumn–winter (May–September). Thus, bottom waters on the continental shelf off Concepcion remain hypoxic throughout the year.

At the inner shelf, hypoxia events were more recurrent at more exposed sites located north of the Gulf of Arauco, such as Chome and Mela, through most of the two years of observation. Sites inside bays, such as Coliumo, Arauco, and Llico, exhibited longer-lasting events in the summer and were not exposed to hypoxia during the winter. Among the seven inner-shelf sites, Arauco showed the most persistent and severe hypoxia, with DO levels well below those observed at the mid-shelf during active upwelling. Arauco also exhibited the greatest contrast between seasons.

The timing of inner-shelf hypoxia events was associated with upwelling-favorable winds in the region. More than half of the hypoxia events detected in our records (59%) occurred after two or fewer days with persistent equatorward wind.

The intense and almost permanent hypoxia in Arauco during summer is likely partly explained by local oxygen consumption, associated with the enhanced productivity and thermal stratification often observed in this section of the Gulf of Arauco in the upwelling season. Excess nutrients and organic matter derived from human activities along this coastal region may further enhance oxygen demand in the sediments and near-bottom waters.

Finally, the climate-driven intensification of upwelling winds in various coastal regions (Sydeman et al., 2014; Rykaczewski et al., 2015) and the strong correlation with increased coastal hypoxia (Aguirre et al., 2021; De La Maza and Farías, 2023) highlight the need to improve the monitoring of DO levels along this and other upwelling coasts.

CRediT authorship contribution statement

Richard Muñoz: Writing – original draft, Writing – review & editing, Data analysis & visualization, Data curation. **Fabián J. Tapia:** Conceptualization, Study design, Funding acquisition, Writing – review & editing, Supervision. **Marcus Sobarzo:** Writing – original draft, Writing – review & editing, Supervision.

Declaration of competing interest

The authors declare that they have no known competing financial interests or personal relationships that could have appeared to influence the work reported in this paper.

Acknowledgments

RM was supported by ANID BECAS/Doctorado Nacional 21231834 and by FONDECYT grant 1161512 awarded to FT. RM also thanks the Laboratory of Coastal Physical Oceanography, Universidad de Concepción for the computer equipment to analyze the data set. FT thanks ANID for the FONDECYT grant (1161512) that made it possible to collect the DO and temperature data series. FT and MS have been partially supported by COPAS Coastal (ANID FB210021) and by INCAR (FONDAP-ANID 1523A0007). MS was also partially supported by the Programa de Investigación sobre Ecosistemas del Golfo de Arauco (PREGA). The COPAS time series program (Departamento de Oceanografía, Universidad de Concepción) provided the monthly hydrographic data from Station 18 (2002–2015).

Data availability

Data will be made available by the authors upon request.

References

Abraham, J.P., Baringer, M., Bindoff, N.L., Boyer, T.P., Cheng, L.J., Church, J.A., Conroy, J.L., Domingues, C.M., Fasullo, J.T., Gilson, J., Goni, G., Good, S.A., Gorman, J.M., Gouretski, V., Ishii, M., Johnson, G.C., Kizu, S., Lyman, J.M., Macdonald, A.M., Minkowycz, W.J., Moffitt, S.E., Palmer, M.D., Piola, A.R., Reseghetti, F., Schuckmann, K., Trenberth, K.E., Velicogna, I., Willis, J.K., 2013. A review of global ocean temperature observations: Implications for ocean heat content estimates and climate change. Rev. Geophys. 51 (3), 450–483. http://dx.doi.org/10.1002/rog.20022.

Adams, K.A., Barth, J.A., Chan, F.T., 2013. Temporal variability of near-bottom dissolved oxygen during upwelling off central Oregon. J. Geophys. Res.: Ocean. 118, 4839–4854. http://dx.doi.org/10.1002/jgrc.20361.

Aguirre, C., Garreaud, R., Belmar, L., Farías, L., Ramajo, L., Barrera, F., 2021. High-frequency variability of the surface ocean properties off central Chile during the upwelling season. Front. Mar. Sci. 8, http://dx.doi.org/10.3389/fmars.2021.702051.

Aguirre Martínez, G., Rudolph, A., Ahumada, R., Loyola, R., Medina, V., 2009. Non-specific toxicity in port sediments: an approach to the content of critical pollutants. Rev. Biol. Mar. y Oceanografía 44, 725–735. http://dx.doi.org/10.4067/S0718-19572009000300018.

Aguirre-Velarde, A., Thouzeau, G., Jean, F., Mendo, J., Cueto-Vega, R., Kawazo-Delgado, M., Vásquez-Spencer, J., Herrera-Sanchez, D., Vega-Espinoza, A., Flye-Sainte-Marie, J., 2019. Chronic and severe hypoxic conditions in Paracas Bay, Pisco, Perú: Consequences on scallop growth, reproduction, and survival. Aquaculture 512, 734259. http://dx.doi.org/10.1016/j.aquaculture.2019.734259.

Ahumada, R., Rudolph, A., Contreras, S., 2004. Evaluation of coastal waters receiving fish processing waste: Lota Bay as a case study. Environ. Monit. Assess. 90 (1), 89–99. http://dx.doi.org/10.1023/B:EMAS.0000003568.37287.ac.

Altieri, A.H., Gedan, K.B., 2015. Climate change and dead zones. Global Change Biol. 21 (4), 1395–1406.

Atkinson, L.P., Valle-Levinson, A., Figueroa, D., De Pol-Holz, R., Gallardo, V.A., Schneider, W., Blanco, J.L., Schmidt, M., 2002. Oceanographic observations in Chilean coastal waters between Valdivia and Concepción. J. Geophys. Res. 107 (C7), 3081. http://dx.doi.org/10.1029/2001JC000991.

Bakun, A., 1990. Global climate change and intensification of coastal ocean upwelling. Science 247 (4939), 198–201. http://dx.doi.org/10.1126/science.247.4939.198.

Bakun, A., Black, B.A., Bograd, S.J., Garcia-Reyes, M., Miller, A.J., Rykaczewski, R.R., Sydeman, W.J., 2015. Anticipated effects of climate change on coastal upwelling ecosystems. Curr. Clim. Chang. Rep. 1, 85–93.

Belmadani, A., Echevín, V., Codron, F., Takahashi, K., Junquas, C., 2013. What dynamics drive future wind scenarios for coastal upwelling off peru and Chile? Clim. Dyn. 43 (7–8), 1893–1914. http://dx.doi.org/10.1007/s00382-013-2015-2.

Booth, J.A.T., McPhee-Shaw, E.E., Chua, P., Kingsley, E., Denny, M., Phillips, R., Bograd, S.J., Zeidberg, L.D., Gilly, W.F., 2012. Natural intrusions of hypoxic, low pH water into nearshore marine environments on the California coast. Cont. Shelf Res. 45, 108–115. http://dx.doi.org/10.1016/j.csr.2012.06.009.

Breitburg, D., Levin, L.A., Oschlies, A., Grégoire, M., Chavez, F.P., Conley, D.J., Garçon, V., Gilbert, D., Gutiérrez, D., Isensee, K., Jacinto, G.S., Limburg, K.E., Montes, I., Naqvi, S.W.A., Pitcher, G.C., Rabalais, N.N., Roman, M.R., Rose, K.A., Seibel, B.A., Telszewski, M., Yasuhara, M., Zhang, J., 2018. Declining oxygen in the global ocean and coastal waters. Science 359 (6371), eaam7240. http://dx.doi.org/10.1126/science.aam7240.

Chan, F.T., Barth, J.A., Blanchette, C.A., Byrne, R.H., Chavez, F., Cheriton, O., Feely, R.A., Friederich, G., Gaylord, B., Gouhier, T., Hacker, S., Hill, T., Hofmann, G., McManus, M.A., Menge, B.A., Nielsen, K.J., Russell, A., Sanford, E., Sevadjian, J., Washburn, L., 2017. Persistent spatial structuring of coastal ocean acidification in the California current system. Sci. Rep. 7 (1), 2526. http://dx.doi.org/10.1038/s41598-017-02777-y.

Chandia, C., Salamanca, M., Hernández, A., Urrutia, R., 2022. Sediment mercury concentration changes as a response to increased industrial activity in Coronel Bay, Chile. Marine Poll. Bull. 178, 113630. http://dx.doi.org/10.1016/j.marpolbul.2022.113630.

Chen, C.-C., Shiah, F.-K., Gong, G.-C., Chen, T.-Y., 2021. Impact of upwelling on phytoplankton blooms and hypoxia along the Chinese coast in the east China sea. Marine Poll. Bull. 167, 112288.

Cid Aguayo, B.E., Vanhulst, J., Rojas, C., 2019. Peasant raw cheese production in the arauco gulf: retro-innovative processes towards socio-ecologically sustainability. Mundo Agrar. 20 (44), e119. http://dx.doi.org/10.24215/15155994e119.

Contreras-Rojas, J., Mardones, P., Sobarzo, M., 2024. Impact of extratropical cyclones on coastal circulation in a semi-enclosed bay within the humboldt current system. EGUsphere [Preprint] http://dx.doi.org/10.5194/egusphere-2024-1822.

Daneri, G., Dellarossa, V., Quiñones, R.A., Jacob, B., Montero, P., Ulloa, O., 2000. Primary production and community respiration in the humboldt current system off Chile and associated oceanic areas. Mar. Ecol. Prog. Ser. 197, 41–49.

De La Maza, L., Farías, L., 2023. The intensification of coastal hypoxia off central Chile: Long term and high frequency variability. Front. Earth Sci. 10, 929271. http://dx.doi.org/10.3389/feart.2022.929271.

Deutsch, C., Ferrel, A., Seibel, B., Pörtner, H.-O., Huey, R.B., 2015. Climate change tightens a metabolic constraint on marine habitats. Science 348 (6239), 1132–1135. http://dx.doi.org/10.1126/science.aaa1605.

Diaz, R.J., 2001. Overview of hypoxia around the world.. J. Environ. Qual. 30 (2), 275–281.

Diaz, R.J., Rosenberg, R., 2008. Spreading dead zones and consequences for marine ecosystems. Science 321 (5891), 926–929. http://dx.doi.org/10.1126/science.115640.

Djurfeldt, L., 1989. Circulation and mixing in a coastal upwelling embayment; Gulf of Arauco, Chile. Cont. Shelf Res. 9 (11), 1003–1016. http://dx.doi.org/10.1016/0278-4343(89)90004-6.

Figueroa, D., Moffat, C., 2000. On the influence of topography in the induction of coastal upwelling along the Chilean coast. Geophys. Res. Lett. 27 (23), 3905–3908.

Fuenzalida, R., Schneider, W., Garcés-Vargas, J., Bravo, L., Lange, C.B., 2009. Vertical and horizontal extension of the oxygen minimum zone in the eastern south Pacific ocean. Deep. Sea Res. Part II: Top. Stud. Ocean. 56 (16), 992–1003. http://dx.doi.org/10.1016/j.dsr2.2008.11.001.

García-Reyes, M., Sydeman, W.J., Schoeman, D.S., Rykaczewski, R.R., Black, B.a., Smit, A.J., Bograd, S.J., 2015. Under pressure: Climate change, upwelling, and eastern boundary upwelling ecosystems. Front. Mar. Sci. 2 (December), 1–10. http://dx.doi.org/10.3389/fmars.2015.00109.

Garcia-Soto, C., Cheng, L., Caesar, L., Schmidtko, S., Jewett, E.B., Cheripka, A., Rigor, I., Caballero, A., Chiba, S., Báez, J.C., Zielinski, T., Abraham, J.P., 2021. An overview of ocean climate change indicators: Sea surface temperature, ocean heat content, ocean pH, dissolved oxygen concentration, arctic sea ice extent, thickness and volume, sea level and strength of the AMOC (atlantic meridional overturning circulation). Front. Mar. Sci. 8, http://dx.doi.org/10.3389/fmars.2021.642372.

González-Saldía, R., Pino-Maureira, N., Muñoz, C., Soto, L., Durán, E., Barra, M., Gutiérrez, S., Díaz, V., Saavedra, A., 2019. Fecal pollution source tracking and thalassogenic diseases: The temporal-spatial concordance between maximum concentrations of human mitochondrial DNA in seawater and hepatitis a outbreaks among a coastal population. Sci. Total Environ. 686, 158–170. http://dx.doi.org/10.1016/j.scitotenv.2019.05.415.

Graham, W.M., Largier, J.L., 1997. Upwelling shadows as nearshore retention sites: the example of northern Monterey bay. Cont. Shelf Res. 17 (5), 509–532.

Grantham, B.A., Chan, F.T., Nielsen, K.J., Fox, D.S., Barth, J.A., Huyer, A., Lubchenco, J., Menge, B.A., 2004. Upwelling-driven nearshore hypoxia signals ecosystem and oceanographic changes. Nature 429, 749–754. http://dx.doi.org/10.1038/nature02605.

Gutiérrez, D., Bouloubassi, I., Sifeddine, A., Purca, S., Goubanova, K., Graco, M., Field, D., Méjanelle, L., Velazco, F., Lorre, A., Salvatteci, R., Quispe, D., Vargas, G., Dewitte, B., Ortlieb, L., 2011. Coastal cooling and increased productivity in the main upwelling zone off Perú since the mid-twentieth century. Geophys. Res. Lett. 38 (7), 1–6. http://dx.doi.org/10.1029/2010GL046324.

Harrison, D., 1989. On climatological monthly mean wind stress and wind stress curl fields over the world ocean. J. Clim. 2 (1), 57–70. http://dx.doi.org/10.1175/1520-0442(1989)002<0057:OCMMWS>2.0.CO;2.

Hernández, A., Tapia, F.J., 2021. Connecting spatial structure in subtidal benthic communities with temporal variability in bottom temperature and dissolved oxygen along an upwelling coast. Estuar. Coast. Shelf Sci. 250, 107166. http://dx.doi.org/10.1016/j.ecss.2021.107166.

Hernández-Miranda, E., Quiñones, R., Aedo, G., Valenzuela, A., Mermoud, N., Román, C., Yañez, F., 2010. A major fish stranding caused by a natural hypoxic event in a shallow bay of the eastern South Pacific Ocean. J. Fish Biol. 76 (7), 1543–1564. http://dx.doi.org/10.1111/j.1095-8649.2010.02580.x.

Hernández-Miranda, E., Veas, R., Labra, F.A., Salamanca, M.A., Quiñones, R.A., 2012. Response of the epibenthic macrofaunal community to a strong upwelling-driven hypoxic event in a shallow bay of the southern Humboldt Current System. Mar. Environ. Res. 79, 16–28. http://dx.doi.org/10.1016/j.marenvres.2012.04.004.

Herrera-Becerril, C.A., Sanchez-Cabeza, J.A., Álvarez Sánchez, L.F., Lara-Cera, A.R., Ruiz-Fernández, A.C., Cardoso-Mohedano, J.G., Machain-Castillo, M.L., Colas, F., 2022. Statistical identification of coastal hypoxia events controlled by wind-induced upwelling. Cont. Shelf Res. 233, http://dx.doi.org/10.1016/j.csr.2021.104634.

Hersbach, H., Bell, B., Berrisford, P., Hirahara, S., Horányi, A., Muñoz-Sabater, J., Nicolas, J., Peubey, C., Radu, R., Schepers, D., et al., 2020. The ERA5 global reanalysis. Q. J. R. Meteorol. Soc. 146 (730), 1999–2049. http://dx.doi.org/10.1002/qj.3803.

Jacob, B.G., Tapia, F.J., Quiñones, R.A., Montes, R., Sobarzo, M.A., Schneider, W., Daneri, G., Morales, C.E., Montero, P., González, H.E., 2018. Major changes in diatom abundance, productivity, and net community metabolism in a windier and dryer coastal climate in the southern Humboldt Current. Prog. Oceanogr. 168, 196–209. http://dx.doi.org/10.1016/j.pocean.2018.10.001.

Johnson, D.R., 1977. Determining vertical velocities during upwelling off the Oregon coast. Deep. Sea Res. 24 (2), 171–180.

Kamykowski, D., Zentara, S.-J., 1990. Hypoxia in the world ocean as recorded in the historical data set. Deep. Sea Res. Part A. Ocean. Res. Pap. 37 (12), 1861–1874.

Kaplan, D.M., Largier, J.L., Navarrete, S.A., Guiñez, R., Castilla, J.C., 2003. Large diurnal temperature fluctuations in the nearshore water column. Estuar. Coast. Shelf Sci. 57, 385–398. http://dx.doi.org/10.1016/S0272-7714(02)00363-3.

Keeling, R.F., Körtzinger, A., Gruber, N., 2010. Ocean deoxygenation in a warming world. Annu. Rev. Mar. Sci. 2 (1), 199–229. http://dx.doi.org/10.1146/annurev.marine.010908.163855.

Kirincich, A.R., Barth, J.A., Grantham, B.A., Menge, B.A., Lubchenco, J., 2005. Wind-driven inner-shelf circulation off central Oregon during summer. J. Geophys. Res. 110 (C10S03), 1–17. http://dx.doi.org/10.1029/2004JC002611.

Largier, J.L., 2020. Upwelling bays: How coastal upwelling controls circulation, habitat, and productivity in bays. Annu. Rev. Mar. Sci. 12, 415–447. http://dx.doi.org/10.1146/annurev-marine-010419-011020.

Levin, L.A., Ekau, W., Gooday, A.J., Jorissen, F., Middelburg, J.J., Naqvi, S.W.A., Neira, C., Rabalais, N.N., Zhang, J., 2009. Effects of natural and human-induced hypoxia on coastal benthos. Biogeosciences 6 (10), 2063–2098. http://dx.doi.org/10.5194/bg-6-2063-2009.

Limburg, K.E., Breitburg, D., Swaney, D.P., Jacinto, G., 2020. Ocean deoxygenation: A primer. One Earth 2 (1), 24–29. http://dx.doi.org/10.1016/j.oneear.2020.01.001.

Linford, P., Pérez-Santos, I., Montero, P., Díaz, P.A., Aracena, C., Pinilla, E., Barrera, F., Castillo, M., Alvera-Azcárate, A., Alvarado, M., Soto, G., Pujol, C., Schwerter, C., Arenas-Uribe, S., Navarro, P., Mancilla-Gutiérrez, G., Altamirano, R., San Martín, J., Soto-Riquelme, C., 2024. Oceanographic processes driving low-oxygen conditions inside patagonian fjords. Biogeosciences 21 (6), 1433–1459. http://dx.doi.org/10.5194/bg-21-1433-2024.

Mardones, P., Wong, Z., Contreras-Rojas, J., Muñoz, R., Hernández-Miranda, E., Sobarzo, M., 2022. Upwelling shadows driven by the low-level jet along the subtropical West Coast of South America: Gulf of Arauco, Chile. J. Geophys. Res.: Ocean. 127 (8), 1–31. http://dx.doi.org/10.1029/2021JC017979.

Merma-Mora, L., Colas, F., Cardich, J., Sánchez, S., Flores, E., Lorenzo, A., Aguirre-Velarde, A., Correa, D., Gutiérrez, D., 2024. Bottom-water hypoxia in the Paracas Bay (Peru, 13.8°S) associated with seasonal and synoptic time scale variability of winds and water stratification. J. Mar. Syst. 241, 103918.

Moffitt, S.E., Moffitt, R.A., Sauthoff, W., Davis, C.V., Hewett, K., Hill, T.M., 2015. Paleoceanographic insights on recent oxygen minimum zone expansion: Lessons for modern oceanography. PLoS One 10 (1), e0115246. http://dx.doi.org/10.1371/journal.pone.0115246.

Paolini-Cuadra, P., Rodríguez, F., Gallardo, C., 2004. Space-time characterization of Punta Lavapié upwelling system through SS NOAA/AVHRR images. Gayana 68 (2), 459–465. http://dx.doi.org/10.4067/S0717-65382004000300026.

Parada, C.E., Sobarzo, M.A., Figueroa, D., Castro, L., 2001. Circulación del Golfo de Arauco en un período de transición estacional: Un nuevo enfoque. Investig. Mar. 29 (1), 11–23. http://dx.doi.org/10.4067/S0717-71782001000100002.

Pizarro, O., Ramírez, N., Castillo, M., Cifuentes, U., Rojas, W., Pizarro-Koch, M., 2015. Underwater glider observations in the oxygen minimum zone off central Chile. Bull. Am. Meteorol. Soc. 97, 1783–1789. http://dx.doi.org/10.1175/BAMS-D-14-00040.1.

Pizarro-Koch, M., Pizarro, O., Dewitte, B., Montes, I., Ramos, M., Paulmier, A., Garçon, V., 2019. Seasonal variability of the southern tip of the oxygen minimum zone in the eastern South Pacific (30-38°S): A modeling study. J. Geophys. Res.: Ocean. 124 (12), 8574–8604. http://dx.doi.org/10.1029/2019JC015201.

Rahn, D.A., Garreaud, R., 2013. A synoptic climatology of the near-surface wind along the west coast of South America. Int. J. Climatol. 34 (3), 780–792. http://dx.doi.org/10.1002/joc.3724.

Ruz, P., Hidalgo, P., Escribano, R., Keister, J., Yebra, L., Franco-Cisterna, B., 2018. Hypoxia effects on females and early stages of calanus chilensis in the humboldt current ecosystem (23°S). J. Exp. Mar. Biol. Ecol. 498, 61–71. http://dx.doi.org/10.1016/j.jembe.2017.09.018.

Rykaczewski, R.R., Dunne, J.P., Sydeman, W.J., García-Reyes, M., Black, B.a., Bograd, S.J., 2015. Poleward displacement of coastal upwelling-favorable winds in the ocean's eastern boundary currents through the 21st century. Geophys. Res. Lett. 42 (15), 6424–6431. http://dx.doi.org/10.1002/2015GL064694.

Sahu, S., Allen, S.E., Saldías, G.S., Klymak, J.M., Zhai, L., 2022. Spatial and temporal origins of the La Perouse low oxygen pool: A combined Lagrangian statistical approach. J. Geophys. Res.: Ocean. 127 (3), http://dx.doi.org/10.1029/2021JC018135, e2021JC018135.

Saldías, G.S., Allen, S.E., 2020. The influence of a submarine canyon on the circulation and cross-shore exchanges around an upwelling front. J. Phys. Oceanogr. 50 (6), 1677–1698. http://dx.doi.org/10.1175/JPO-D-19-0130.1.

Saldías, G.S., Ramos-Musalem, K., Allen, S.E., 2021. Circulation and upwelling induced by coastal trapped waves over a submarine canyon in an idealized eastern boundary margin. Geophys. Res. Lett. 48 (11), http://dx.doi.org/10.1029/2021GL093548, e2021GL093548.

Schmidtko, S., Stramma, L., Visbeck, M., 2017. Decline in global oceanic oxygen content during the past five decades. Nature 542 (7641), 335–339. http://dx.doi.org/10.1038/nature21399.

Schneider, W., Donoso, D., Garcés-Vargas, J., Escribano, R., 2017. Water-column cooling and sea surface salinity increase in the upwelling region off central-south Chile driven by a poleward displacement of the South Pacific High. Prog. Oceanogr. 151, 38–48. http://dx.doi.org/10.1016/j.pocean.2016.11.004.

Silva, G.M.e., Campos, D.F., Brasil, J.A.T., Tremblay, M., Mendiondo, E.M., Ghiglieno, F., 2022. Advances in technological research for online and in situ water quality monitoring—A review. Sustainability 14 (9), 5059.

Silva, N., Vargas, C.A., 2014. Hypoxia in Chilean patagonian fjords. Prog. Oceanogr. 129, 62–74. http://dx.doi.org/10.1016/j.pocean.2014.05.016.

Sobarzo, M.A., Bravo, L., Donoso, D., Garcés-Vargas, J., Schneider, W., 2007. Coastal upwelling and seasonal cycles that influence the water column over the continental shelf off central Chile. Prog. Oceanogr. 75, 363–382. http://dx.doi.org/10.1016/j.pocean.2007.08.022.

Sobarzo, M.A., Bravo, L., Moffat, C., 2010. Diurnal-period, wind-forced ocean variability on the inner shelf off Concepción, Chile. Cont. Shelf Res. 30, 2043–2056. http://dx.doi.org/10.1016/j.csr.2010.10.004.

Sobarzo, M., Djurfeldt, L., 2004. Coastal upwelling process on a continental shelf limited by submarine canyons, Concepción, central Chile. J. Geophys. Res.: Ocean. 109 (C12), 1–20. http://dx.doi.org/10.1029/2004JC002350.

Sobarzo, M.A., Saldías, G.S., Tapia, F.J., Bravo, L., Moffat, C., Largier, J.L., 2016. On subsurface cooling associated with the Biobío River Canyon (Chile). J. Geophys. Res.: Ocean. 121 (7), 4568–4584. http://dx.doi.org/10.1002/2016JC011796.

Sydeman, W.J., García-Reyes, M., Schoeman, D.S., Rykaczewski, R.R., Thompson, S.A., Black, B.A., Bograd, S.J., 2014. Climate change and wind intensification in coastal upwelling ecosystems. Science 345, 77–80. http://dx.doi.org/10.1126/science.1251635.

Tapia, F.J., Largier, J.L., Castillo, M.I., Wieters, E.A., Navarrete, S.A., 2014. Latitudinal discontinuity in thermal conditions along the nearshore of central-northern Chile. PLoS ONE http://dx.doi.org/10.1371/journal.pone.0110841.

Tapia, F.J., Navarrete, S.A., Castillo, M.I., Menge, B.A., Castilla, J.C., Largier, J.L., Wieters, E.A., Broitman, B.R., Barth, J.A., 2009. Thermal indices of upwelling effects on inner-shelf habitats. Prog. Oceanogr. 83, 278–287. http://dx.doi.org/10.1016/j.pocean.2009.07.035.

Testa, G., Masotti, I., Farias, L., 2018. Temporal variability in net primary production in an upwelling area off central Chile (36°S). Front. Mar. Sci. 5, 179. http://dx.doi.org/10.1371/journal.pone.0110841.

Thiel, M., Macaya, E.C., Acuña, E., Arntz, W.E., Bastias, H., Brokordt, K.B., Camus, P.A., Castilla, J.C., Castro, L.R., Cortes, M., Dumont, C.P., Escribano, R., Fernández, M., Gajardo, J., Gaymer, C.F., Gomez, I., Gonzalez, A.E., González, H.E., Haye, P.A., Illanes, J.-E., Iriarte, J.L., Lancellotti, D.A., Luna-Jorquera, G., Luxoro, C., Manríquez, P.H., Marin, V.H., Muñoz, P., Navarrete, S.A., Perez, E., Poulin, E., Sellanes, J., Sepúlveda, H.H., Stotz, W., Tala, F., Thomas, A.C., Vargas, C.A., Vasquez, J.A., Vega, J.M.A., 2007. The Humboldt current system of northern and central Chile: Oceanographic processes, ecological interactions and socioeconomic feedback. Ocean. Mar. Biol: Annu. Rev. 45, 195–344. http://dx.doi.org/10.1201/9781420050943.ch6.

Trenberth, K.E., 1990. Recent observed interdecadal climate changes in the Northern Hemisphere. Bull. Am. Meteorol. Soc. 71 (7), http://dx.doi.org/10.1175/1520-0477(1990)071<0988:ROICCI>2.0.CO;2, 998–993.

Valle-Levinson, A., Atkinson, L.P., Castro, L.R., 2003. Flow induced by upwelling winds in an equatorward facing bay: Gulf of Arauco, Chile. J. Geophys. Res. 108, 1–14. http://dx.doi.org/10.1029/2001JC001272.

Vargas, G., Pantoja, S., Rutllant, J.A., Lange, C.B., Ortlieb, L., 2007. Enhancement of coastal upwelling and interdecadal ENSO-like variability in the Perú-Chile Current since late 19th century. Geophys. Res. Lett. http://dx.doi.org/10.1029/2006GL028812.

Vergara, O.A., Figueroa, P.A., Salas, C., Vásquez, S.I., Muñoz, R., Saldías, G.S., 2024. The influence of the biobio canyon on the circulation and coastal upwelling/downwelling off central Chile. Cont. Shelf Res. 105335. http://dx.doi.org/10.1016/j.csr.2024.105335.

Walter, R.K., Huie, S.A., Abraham, J.C.P., Pasulka, A., Davis, K.A., Connolly, T.P., Mazzini, P.L., Robbins, I., 2022. Seasonal controls on nearshore dissolved oxygen variability and hypoxia in a coastal embayment. Estuar. Coast. Shelf Sci. 278, 108123. http://dx.doi.org/10.1016/j.ecss.2022.108123.

Walter, R.K., Woodson, C.B., Leary, P.R., Monismith, S.G., 2014. Connecting wind-driven upwelling and offshore stratification to nearshore internal bores and oxygen variability. J. Geophys. Res.: Ocean. 119, 3517–3534. http://dx.doi.org/10.1002/2014JC009998.

Weidberg, N., Ospina-Alvarez, A., Bonicelli, J., Barahona, M., Aiken, C.M., Broitman, B.R., Navarrete, S.A., 2020. Spatial shifts in productivity of the coastal ocean over the past two decades induced by migration of the Pacific Anticyclone and Bakun's effect in the humboldt upwelling ecosystem. Glob. Planet. Change 193, 103259. http://dx.doi.org/10.1016/j.gloplacha.2020.103259.

Winckler Grez, P., Aguirre, C., Farías, L., Contreras-López, M., Masotti, Í., 2020. Evidence of climate-driven changes on atmospheric, hydrological, and oceanographic variables along the Chilean coastal zone. Clim. Change 163 (2), 633–652. http://dx.doi.org/10.1007/s10584-020-02805-3.

Wong, Z., Saldías, G.S., Largier, J.L., Strub, P.T., Sobarzo, M., 2021. Surface thermal structure and variability of upwelling shadows in the Gulf of Arauco, Chile. J. Geophys. Res.: Ocean. 126, http://dx.doi.org/10.1029/2020JC016194.

Woodson, C.B., Eerkes-Medrano, D., Flores-Morales, A., Foley, M.M., Henkel, S.K., Hessing-Lewis, M., Jacinto, D., Needles, L., Nishizaki, M.T., O'Leary, J., Ostrander, C.E., Pespeni, M., Schwager, K.B., Tyburczy, J.A., Weersing, K.A., Kirincich, A.R., Barth, J.A., Mcmanus, M.A., Washburn, L., 2007. Local diurnal upwelling driven by sea breezes in northern Monterey Bay. Cont. Shelf Res. 27, 2289–2302. http://dx.doi.org/10.1016/j.csr.2007.05.014.